

NACA RM L52D21a

7325

NACA

RESEARCH MEMORANDUM

AN ANALYSIS OF THE PRESSURE DISTRIBUTION MEASURED ON A
BODY OF REVOLUTION AT TRANSONIC SPEEDS IN THE
SLOTTED TEST SECTION OF THE LANGLEY
8-FOOT TRANSONIC TUNNEL

By Bruce B. Estabrooks

Langley Aeronautical Laboratory
Langley Field, Va.

CLASSIFIED DOCUMENT

NATIONAL ADVISORY COMMITTEE
FOR AERONAUTICS

WASHINGTON

June 25, 1952



*Receipt signed
general*

Classification cancelled (or changed to) Unclassified
By Authority of New Tech Pub Announcement #79
(OFFICIAL USE) (SEE TO CHANGE)

By
NAME AND

10 Apr 56

MK

.....
GRADE OF OFFICER MAKING CHANGE

6 Apr 61
DATE



NATIONAL ADVISORY COMMITTEE FOR AERONAUTICS

RESEARCH MEMORANDUM

AN ANALYSIS OF THE PRESSURE DISTRIBUTION MEASURED ON A
BODY OF REVOLUTION AT TRANSONIC SPEEDS IN THE
SLOTTED TEST SECTION OF THE LANGLEY
8-FOOT TRANSONIC TUNNEL

By Bruce B. Estabrooks

SUMMARY

The pressure distributions reported in NACA RM L51F05 are analyzed in this paper for the effects of Mach number and angle of attack on normal force, pitching moment, and pressure drag. The results obtained from the pressure-distribution data indicate that the normal-force and pitching-moment characteristics of the body of revolution were nearly independent of Mach number effects at moderate angles of attack. A marked increase in pressure drag occurred at all angles of attack when the Mach number was increased above 0.99. The positive loading on the body increased considerably over the forward sections and spread rearward with increase in angle of attack from 8° to 20° at all Mach numbers. The center of pressure of the body moved rearward with increase in angle of attack, and its location was nearly independent of Mach number effects. The normal-force and pitching-moment characteristics predicted by the theoretical method of NACA RM A9I26 are in fair agreement with the experimental results of this report at the lower angles of attack. Separation of the flow over the upper surface of the body caused the experimental characteristics to deviate from the theoretical characteristics in the high angle-of-attack range of 12° to 20° .

INTRODUCTION

During the last several years a number of papers have been published, references 1 to 4, which present and analyze the pressures about various bodies of revolution in both the subsonic and supersonic speed ranges. There has, however, been little or no wind-tunnel data presented in the transonic speed range because of the lack of such a test facility. Recent

modifications (ref. 5) of the Langley 8-foot transonic tunnel test section have made it possible to obtain aerodynamic data at Mach numbers through the speed of sound without the usual effects of choking and blockage. The pressure distribution on a body of revolution was investigated in this transonic test section at Mach numbers through the transonic speed range for various angles of attack. The pressure distributions obtained have been presented in reference 6 with a brief discussion of the more significant indications obtained from these basic pressure distributions. A more complete analysis of the pressure distributions was undertaken here to provide a further understanding of the characteristics of transonic flow.

SYMBOLS

A	body frontal area
d	body section diameter
d_{\max}	body maximum section diameter
l	length of body sections parallel to the vertical plane of symmetry
\bar{l}	average length of body sections parallel to the vertical plane of symmetry
L	total length of body
M	free-stream Mach number
p	local static pressure
p_0	free-stream static pressure
P	pressure coefficient, $\frac{p - p_0}{q}$
P_{av}	average pressure coefficient of a body cross section
$P_{\alpha=0}$	pressure coefficient at zero angle of attack
ΔP	incremental pressure coefficient due to angle of attack, $P - P_{\alpha=0}$

q	free-stream dynamic pressure, $\frac{1}{2}\rho V^2$
R	Reynolds number, $\frac{\rho V L}{\mu}$
r	body section radius
V	free-stream velocity
x	distance measured along longitudinal axis of body
y	distance measured perpendicular to vertical plane of symmetry
α	angle of attack of body center line
θ	model cylindrical coordinate
ρ	free-stream mass density
μ	free-stream coefficient of viscosity
η	ratio of the drag coefficient of a circular cylinder of finite length to that of a cylinder of infinite length (note ref. 7)

The coefficients are defined as follows:

c_{dc}	drag coefficient which would be experienced by a circular cylinder section of radius r at Reynolds number and Mach number based upon the diameter and the cross component of velocity (note ref. 7)
c_n	body cross-section normal-force coefficient, $\frac{1}{2r} \int_{-r}^r (P_L - P_U) dy$
c_{ns}	body longitudinal section normal-force coefficient, $\frac{1}{l} \int_0^l (P_L - P_U) dx$
C_N	normal-force coefficient based on body frontal area

C_m body pitching-moment coefficient about 60 percent body station based on body frontal area and body total length

C_{Dp} pressure-drag coefficient based on body frontal area

Subscripts:

cr critical

L lower surface of body ($\theta = 270^\circ \rightarrow 0^\circ \rightarrow 90^\circ$)
(note fig. 2)

U upper surface of body ($\theta = 90^\circ \rightarrow 180^\circ \rightarrow 270^\circ$)
(note fig. 2)

s body longitudinal section

APPARATUS AND METHODS

Tunnel

The pressure-distribution investigation was conducted in the Langley 8-foot transonic tunnel, which is a dodecagonal, slotted-throat, single-return wind tunnel designed for continuous operation through the speed of sound up to a Mach number of 1.13, reference 5. The flow was uniform in the vicinity of the model throughout the speed range. Deviations from the free-stream Mach number in the region occupied by the model did not exceed 0.003 at Mach numbers up to 1.02. At Mach numbers from 1.11 to 1.13 the deviations did not exceed 0.008 (ref. 8). The flow in the tunnel had an angularity of 0.10° and all data were obtained at angles of attack which compensated for this angularity.

Model

The body of revolution was designed with the ordinates of the general transonic fuselage and is the same model used in the investigation reported in reference 1. The model had circular cross sections and a basic fineness ratio of 12, although an actual fineness ratio of 10 was obtained after cutting off the rear one-sixth of the body to attach the sting. The model ordinates are presented in figure 1. Static-pressure orifices were distributed along six meridians on the body, as shown in figure 2. The average Reynolds number, figure 3, for this investigation varied from 9.28×10^6 to 11.23×10^6 when based on the total body length of 33.333 inches.

~~CONFIDENTIAL~~

Reduction of Data

The pressure-coefficient data for the Mach numbers and angles of attack covered in this report have been presented in reference 6. The pressure coefficients for the body of revolution are estimated to be accurate within ± 0.006 . The angle of attack of the model was measured to within $\pm 0.10^\circ$ by a cathetometer.

At Mach numbers from 1.02 to 1.11, the effects of reflected disturbance waves on the model surface pressure become significant. Accordingly, no data were taken in that Mach number range; in the final plots of the results (figs. 12, 14, 16, and 17) the curves are shown as dashed lines in this range of Mach numbers.

The normal-force, pitching-moment, and pressure-drag coefficients were obtained from integrations of the experimental pressure-coefficient data. It was assumed that the pressure distributions were symmetrical about the body for these integrations. The theoretical cross-section normal-force coefficients, normal-force coefficients, pitching-moment coefficients, and center-of-pressure location have been computed by the method of reference 7. Average values of $\eta = 0.68$ and $cd_c = 1.2$, selected from figures of reference 7, were used for the theoretical calculations.

RESULTS AND DISCUSSION

Pressure Distributions

Zero angle of attack.- Referring to the pressure distributions, figure 4, it is noted that increasing the Mach number from 0.89 to 0.97 increased the level of the negative pressure coefficients along the body. At the Mach number of 0.97, supersonic velocities are indicated along the body from the 25-percent-body-length position to approximately the 85-percent-body-length position. With the Mach number increased to 0.99, the presence of a shock is indicated at approximately the 87-percent-body-length position by the rapid increase in pressure coefficient at the beginning of the region of compression near the base of the model. With increase in Mach number to 1.02, the shock moved downstream to approximately the 91 percent body station and the region of the body affected by local supersonic flow increased. Further increases in Mach number to 1.11 and 1.13 resulted in a continued rearward movement of the shock on the model and rearward spread of the region of negative pressure coefficients. At the same time the level of the negative pressure coefficients decreased.

~~CONFIDENTIAL~~

~~CONFIDENTIAL~~

Angle of attack.- The pressure distributions along the body for a Mach number of 0.99 and an angle of attack range from 4° to 20° are presented in figure 5 in order to illustrate the effect of angle-of-attack variation on the pressure distributions at a constant Mach number. When the angle of attack was increased from 4° to 20° , the level of the negative pressure coefficients over the upper surface of the rear section of the body remained relatively high. This independence of the negative pressure coefficients over the rearward sections to angle-of-attack change is indicative of flow separation. The pressure coefficients over the upper surface of the nose became more negative with increase in angle of attack and at the same time, the region of supersonic flow over the upper surface spread forward. The pressure coefficients over the lower surface in the vicinity of the 0° meridian of the nose of the body became more positive and the rate of pressure drop along the lower surface (0° meridian) of the body from the nose to the region of compression at the rear sections increased when the angle of attack increased from 4° to 20° at all of the Mach numbers.

In order to illustrate the effect of Mach number on the pressure distributions at constant angle of attack, the pressure distributions for an angle of attack of 8° at several representative Mach numbers are presented in figure 6. Indication of supercritical conditions of local flow over most of the central portion of the body at a Mach number of 0.97 may be seen in figure 6(a). When the Mach number was increased to 0.99, figure 6(b), the supersonic region over the body increased and a negative pressure coefficient peak developed over the lower surface in the region of expansion upstream of the shock. The shock is recognizable from the pressure distributions at the upstream extremity of the region of compression near the base of the model. As the Mach number was increased to 1.02, figure 6(c), the level of the negative pressure coefficients over the rear of the body increased and the shock that terminated the region of relatively high negative pressure coefficients moved rearward. With increase in Mach number to 1.11, figure 6(d), the shock continued to move downstream and the region of negative pressure coefficients spread rearward. Increasing the Mach number above 1.02 decreased the level of the negative pressure coefficients, although the region of the body affected by local supersonic flow increased.

The incremental pressure coefficients due to angle of attack obtained from the experimental pressure distributions are compared with the theoretical incremental pressure coefficients obtained by the method of reference 9 in figure 7 as a function of the angular coordinate around the body. The incremental pressure coefficient is defined as the change in value of the pressure coefficient at any station resulting from the variation of angle of attack from 0° . The incremental pressure data are presented for all angles of attack at several representative body stations and Mach numbers. The experimental incremental-pressure data

~~CONFIDENTIAL~~

at all angles of attack were generally independent of Mach number as predicted by theory. The presence of a shock in the vicinity of the 91.5 percent body station at a Mach number of 1.02 caused the experimental incremental pressure coefficients at this station and Mach number to vary from the values indicated at the other Mach numbers and predicted by theory.

The incremental pressure coefficients on the lower surface of the body are in good agreement with the theory for the angles of attack presented. The theory indicates that the pressure recovery over the upper surface of the body increases where the section radii are decreasing with distance along the body and as the angle of attack increases. In figure 7(a), an indication of cross-flow separation, characterized by the incremental-pressure-coefficient gradient of the experimental data becoming nearly zero, is noted over the upper surface at the 91.5 percent body station. As the angle of attack was increased to 8° , figure 7(b), the region of separated flow moved forward to the 73.5 percent body station and downward along the sides of the body toward the 90° cylindrical coordinate position at the 91.5 percent body station. At an angle of attack of 12° , figure 7(c), the cross-flow separation moved forward along the body to the vicinity of the 61.5-percent body station. The incremental pressure distributions in figure 7(d) indicate that the region of cross-flow separation moved forward to the vicinity of the nose of the body and downward to the vicinity of the 75° cylindrical coordinate position over the rear half of the body. The subsequent decrease in incremental pressure coefficients to less than that predicted by theory over the top side of the body is associated with the formation of vorticity over the upper surface of the body. Previous investigations have established the fact that two symmetrically disposed vortices are formed on the upper side of bodies of revolution at moderate angles of attack with the vortex cores aligned approximately with the free air stream, reference 2.

Loading Characteristics

Lateral load distributions.— The lateral load distributions over the body are presented in figure 8. The longitudinal-section normal-force coefficients were obtained for six sections parallel to the model vertical plane of symmetry. For the Mach numbers investigated, as the angle of attack was increased to 20° , the loading over the inboard region of the body was increased by approximately equal increments. At the same time the outboard regions of the body experienced a decrease in loading which became negative at an angle of attack of 8° for Mach numbers from 0.89 to 1.02 and at an angle of attack of 12° for Mach numbers of 1.11 and 1.13. The increase of the loading over the inboard region of the body with increase in angle of attack was contributed to by the trend toward more

positive pressure coefficients on the lower surface (0° meridian) of the nose and the increase in negative pressure coefficients in the region of the 180° meridian.

Longitudinal load distributions.— The longitudinal load distributions for all of the Mach numbers, figure 9, indicate that the loading over the forward section of the body increased and the region of positive loading shifted rearward with increase in angle of attack from 8° to 20° . The increase of the load over the fuselage forward sections was associated with the same trends of the pressure coefficients over the forward sections noted in the discussion of the lateral load distributions. The spread of the region of separated flow over the central sections of the body upper surface with increase in angle of attack contributed to the rearward spread of the region of positive loading over the body.

Center of pressure.— The increase and rearward spread of the positive load over the model along with the essentially constant negative load over the rear of the model with increase in angle of attack for all of the Mach numbers resulted in a rearward shift of the center of pressure of the load as shown in figure 10. As the angle of attack was increased from 4° to 20° , the center of pressure moved from a position approximately 28 percent body length in front of the body to a position 26 percent body length behind the nose of the body. The experimental locations of the center of pressure were slightly more rearward of the location predicted by theory. The center of pressure varied a maximum of 10 percent and 5 percent body length at angles of attack of 4° and 8° , respectively, over the Mach number range. Mach number effects at angles of attack of 12° and 20° were negligible.

Normal-Force Characteristics

The longitudinal distributions of the cross-sectional normal-force coefficients are presented in figure 11 along with the corresponding theoretical coefficients computed by the method of reference 7. Mach number effects on the cross-sectional normal-force coefficients were negligible for all the body sections except where the presence of the local shock caused variations in the normal-force coefficients for sections near the model base.

The experimental cross-sectional normal-force distributions agree very well with the distributions predicted by the method of reference 7 at angles of attack up to 12° , except where separation of the flow over the upper surface of the body existed. At the highest angle of attack of 20° , the predicted normal-force coefficients were more positive over the forward sections of the body than the experimental normal-force

coefficients. This resulted from the theoretical assumption that the cross-flow drag coefficient c_{d_c} was constant along the body, whereas the experimental cross-flow drag coefficient probably varied from nearly zero at the nose to a value greater than the theoretical cross-flow drag coefficient over the rearward sections of the body due to separated flow conditions over the model upper surface.

The variation of normal-force coefficient with Mach number and angle of attack is presented in figure 12. The normal-force coefficients, based on body frontal area, were obtained by integration of the longitudinal loading curves, figure 9. The normal-force coefficients obtained from the investigation of this body in the solid-nozzle test section of the Langley 8-foot transonic tunnel (ref. 1) are also shown in figure 12. The discrepancies between the normal-force coefficients of the two investigations may have been caused to some extent by differences in surface conditions of the body affecting the extent of the separated-flow region. The normal-force coefficient for the body exhibited little change with increase in Mach number through the transonic speed range for the angle-of-attack range investigated. The normal-force coefficient at constant angle of attack varied a maximum of 0.04 at angles of attack from 4° to 12° and increased from 0.87 to 1.03 at an angle of attack of 20° with increase in Mach number through the transonic speed range.

The normal-force coefficients for the Mach numbers investigated are compared with the theoretical normal-force coefficients as a function of angle of attack in figure 13. For the Mach numbers investigated, the slope of the normal-force curve remained nearly constant in the range of angles of attack from 8° to 20° . The experimental normal-force coefficients were adequately predicted by the theory at all Mach numbers for 4° angle of attack. As the angle of attack was increased to 12° and 20° , the effect of assuming a constant cross-flow drag coefficient c_{d_c} along the body in the theoretical calculation contributed to an overestimation of the normal force. At an angle of attack of 20° , the predicted normal-force coefficient was as much as 0.30 more positive than that obtained from experiment.

The normal-force coefficients obtained from a pressure-distribution investigation on this body and a force investigation of a similar model in the solid-nozzle test section of the Langley 8-foot high-speed tunnel have been compared in reference 1. Since it has been concluded in reference 1 that the normal-force results obtained from the two types of investigations are in good agreement, no comparisons have been made herein.

Pitching-Moment Characteristics

The variation with Mach number of the pitching-moment coefficients of the body is presented in figure 14. The pitching-moment coefficients, with the axis of moments at the 60 percent body station, are based on the frontal area and the total length of the body. Also shown in figure 14 are the pitching-moment coefficients of the body obtained from reference 1 for angles of attack from 4° to 12° and Mach numbers from 0.60 to 0.96 and a supersonic Mach number of 1.2. The discrepancies between the pitching-moment coefficients of the two investigations may have been caused by differences in surface conditions of the body affecting the extent of the separated flow region. Since reference 1 included comparisons between the pitching-moment coefficients obtained from a pressure investigation and a force investigation on a similar body of revolution and concluded that there is good agreement between the results obtained from the two types of investigations, no comparisons have been made herein.

Mach number effects on the pitching-moment coefficients were small through the transonic speed range. As shown in figure 14, the maximum variations with Mach number in pitching-moment coefficient are 0.02 at constant angle of attack between 4° and 12° and 0.03 at an angle of attack of 20° .

The variation with angle of attack of the experimental pitching-moment coefficients for all the Mach numbers is presented in figure 15. The pitching-moment coefficients became more positive with increase in angle of attack from 4° to 20° because of the increase in load over the forward section of the body with increase in angle of attack noted in the discussion of the longitudinal load distributions, figure 9. The variation of the slope of the pitching-moment curve was negligible for all Mach numbers. The theoretical pitching-moment coefficients calculated by the method of reference 7 are also presented in figure 15. The theory predicted the pitching moment within reasonable accuracy at angles of attack of 4° and 8° , but as the angle of attack was increased to 20° , the theory overestimated the pitching-moment coefficient by a maximum of 0.06.

Drag Characteristics

The variation with Mach number of the body pressure drag at all of the angles of attack is presented in figure 16. The pressure drag data of reference 1 are also shown in figure 16.

The body-pressure-drag-coefficient variation at all of the angles of attack was small (0.02 maximum) with increase in Mach number from 0.89 to 0.99. As the Mach number was increased from 0.99 to 1.02, a substantial

increase in pressure-drag coefficient occurred at all the angles of attack. This increase in pressure drag was due to the positive trend of the pressure coefficients over the nose of the body, the increase in the level of the negative pressure coefficients over the rear of the body, and the rearward movement of the local shock located near the base of the model. As the Mach number was increased from 1.02 to 1.13, the body pressure drag increased slightly at all the angles of attack, but without the abruptness noted with the increase in Mach number from 0.99 to 1.02. The slight increase in pressure drag at Mach numbers above 1.02 was associated with the rearward movement toward the model base of the local shock and rearward spread of the region of negative pressure coefficients.

The body pressure-drag coefficients at zero angle of attack are compared in figure 17 with the pressure drag obtained from free-fall tests, reference 3. Also presented in figure 17 are the pressure-drag coefficients of the forebody (the portion of the body forward of the maximum body diameter). The body pressure-drag coefficients obtained from the two investigations are nearly zero at Mach numbers from 0.89 to 0.99. Both investigations indicate that the body pressure-drag coefficients increased abruptly when the Mach number was increased above 0.99 with the free-fall body pressure-drag coefficients increasing approximately 0.020 more than the tunnel pressure-drag coefficients at Mach numbers of 1.02 and above. The discrepancies between the body drag coefficients at Mach numbers from 0.99 to 1.02 may be due to the effect of the reflected shock slightly upstream of the maximum-thickness region of the body (ref. 8). The drag differences at Mach numbers of 1.11 and 1.13 could be attributed to differences in body shape or to possible inadequacies in sting-support tare corrections.

The pressure-drag coefficients of the body and the forebody were approximately zero at Mach numbers from 0.89 to 0.99. When the Mach number was increased to 1.02, the forebody was responsible for 60 percent of the total rise in body pressure drag. At Mach numbers above 1.02, the forebody pressure drag remained nearly constant while the body pressure drag continued to increase slightly. The increase of body pressure drag above 1.02 was contributed to by the rearward spread of the region of negative pressure coefficients over the rear sections of the body with increase in Mach number.

CONCLUSIONS

The results of the pressure-distribution investigation of a body of revolution of fineness ratio 10 indicate that:

1. The body pressure-drag coefficient increased considerably with increase in Mach number from 0.99 to 1.02 at all angles of attack. At 0° angle of attack the forebody was responsible for approximately 60 percent of the total rise in body pressure drag as the Mach number was increased from 0.99 to 1.02.

2. The positive loading on the body increased considerably over the forward sections of the body and spread rearward with increase in angle of attack from 8° to 20° at all Mach numbers.

3. The body center of pressure shifted rearward from a position approximately 28 percent body length in front of the nose to a position 26 percent body length behind the nose with increase in angle of attack from 4° to 20° . The location of the center of pressure was nearly independent of Mach number effects.

4. The lateral load distributions on the body exhibited a large increase in loading over the inboard region and a decrease in loading over the outboard region of the body with increase in angle of attack from 4° to 20° at all Mach numbers.

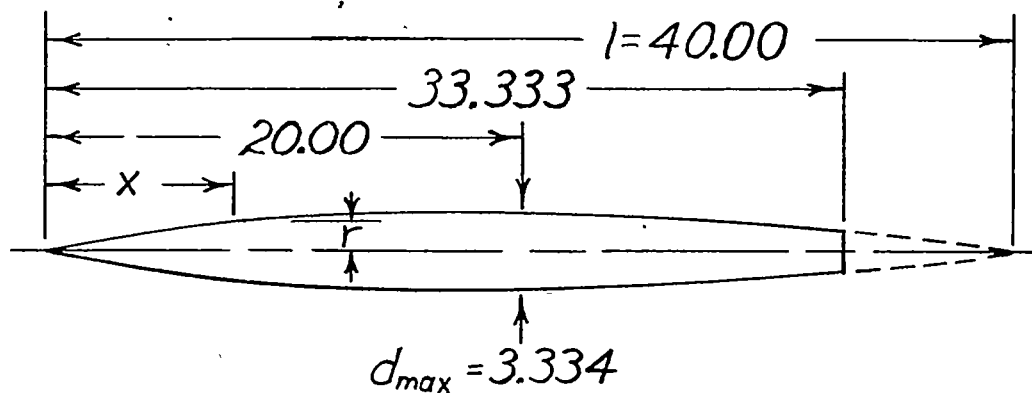
5. The normal-force and pitching-moment characteristics predicted by the theoretical method of NACA RM A9126 are in fair agreement with the results of this investigation at the lower angles of attack. Separation of the flow over the body upper surface caused some discrepancies between the theoretical and experimental characteristics in the high angle-of-attack range of 12° to 20° .

6. Normal-force and pitching-moment characteristics of this body remained relatively constant with increase in Mach number through the transonic speed range at low angles of attack. At 20° angle of attack maximum variations of 0.16 in normal-force coefficient and 0.03 in pitching-moment coefficient occurred with increase in Mach number from 0.89 to 1.12.

Langley Aeronautical Laboratory
National Advisory Committee for Aeronautics
Langley Field, Va.

REFERENCES

1. Loving, Donald L., and Estabrooks, Bruce B.: Transonic-Wing Investigation in the Langley 8-Foot High-Speed Tunnel at High Subsonic Mach Numbers and at a Mach Number of 1.2. Analysis of Pressure Distribution of Wing-Fuselage Configuration Having a Wing of 45° Sweepback, Aspect Ratio 4, Taper Ratio 0.6, and NACA 65A006 Airfoil Section. NACA RM L51F07, 1951.
2. Luidens, Roger W., and Simon, Paul C.: Aerodynamic Characteristics of NACA RM-10 Missile in 8- by 6-Foot Supersonic Wind Tunnel at Mach Numbers From 1.49 to 1.98. I - Presentation and Analysis of Pressure Measurements (Stabilizing Fins Removed). NACA RM E50D10, 1950.
3. Thompson, Jim Rogers: Measurements of the Drag and Pressure Distribution on a Body of Revolution Throughout Transition From Subsonic to Supersonic Speeds. NACA RM L9J27, 1950.
4. Matthews, Clarence W.: A Comparison of the Experimental Subsonic Pressure Distributions About Several Bodies of Revolution With Pressure Distributions Computed by Means of the Linearized Theory. NACA TN 2519, 1952. (Supersedes NACA RM L9F28.)
5. Wright, Ray H., and Ritchie, Virgil S.: Characteristics of a Transonic Test Section With Various Slot Shapes in the Langley 8-Foot High-Speed Tunnel. NACA RM L51H10, 1951.
6. Loving, Donald L., and Williams, Claude V.: Basic Pressure Measurements on a Fuselage and a 45° Sweptback Wing-Fuselage Combination at Transonic Speeds in the Slotted Test Section of the Langley 8-Foot High-Speed Tunnel. NACA RM L51F05, 1951.
7. Allen, H. Julian: Estimation of the Forces and Moments Acting on Inclined Bodies of Revolution of High Fineness Ratio. NACA RM A9I26, 1949.
8. Ritchie, Virgil S., and Pearson, Albin O.: Calibration of the Slotted Test Section of the Langley 8-Foot Transonic Tunnel and Preliminary Experimental Investigation of Boundary-Reflected Disturbances. NACA RM L51K14, 1952.
9. Allen, H. Julian: Pressure Distribution and Some Effects of Viscosity on Slender Inclined Bodies of Revolution. NACA TN 2044, 1950.



ORDINATES			
x/l	r/l	x/l	r/l
0	0		
.0050	.00231	.4500	.041143
.0075	.00298	.5000	.04167
.0125	.00428	.5500	.04130
.0250	.00722	.6000	.04024
.0500	.01205	.6500	.03842
.0750	.01613	.7000	.03562
.1000	.01971	.7500	.03128
.1500	.02593	.8000	.02526
.2000	.03090	.8333	.02083
.2500	.03465	.8500	.01852
.3000	.03741	.9000	.01125
.3500	.03933	.9500	.00439
.4000	.04063	1.0000	0
L.E. radius = 0.00057			
NACA			

Figure 1.- Details of body of fineness ratio 10. All dimensions are in inches.



15

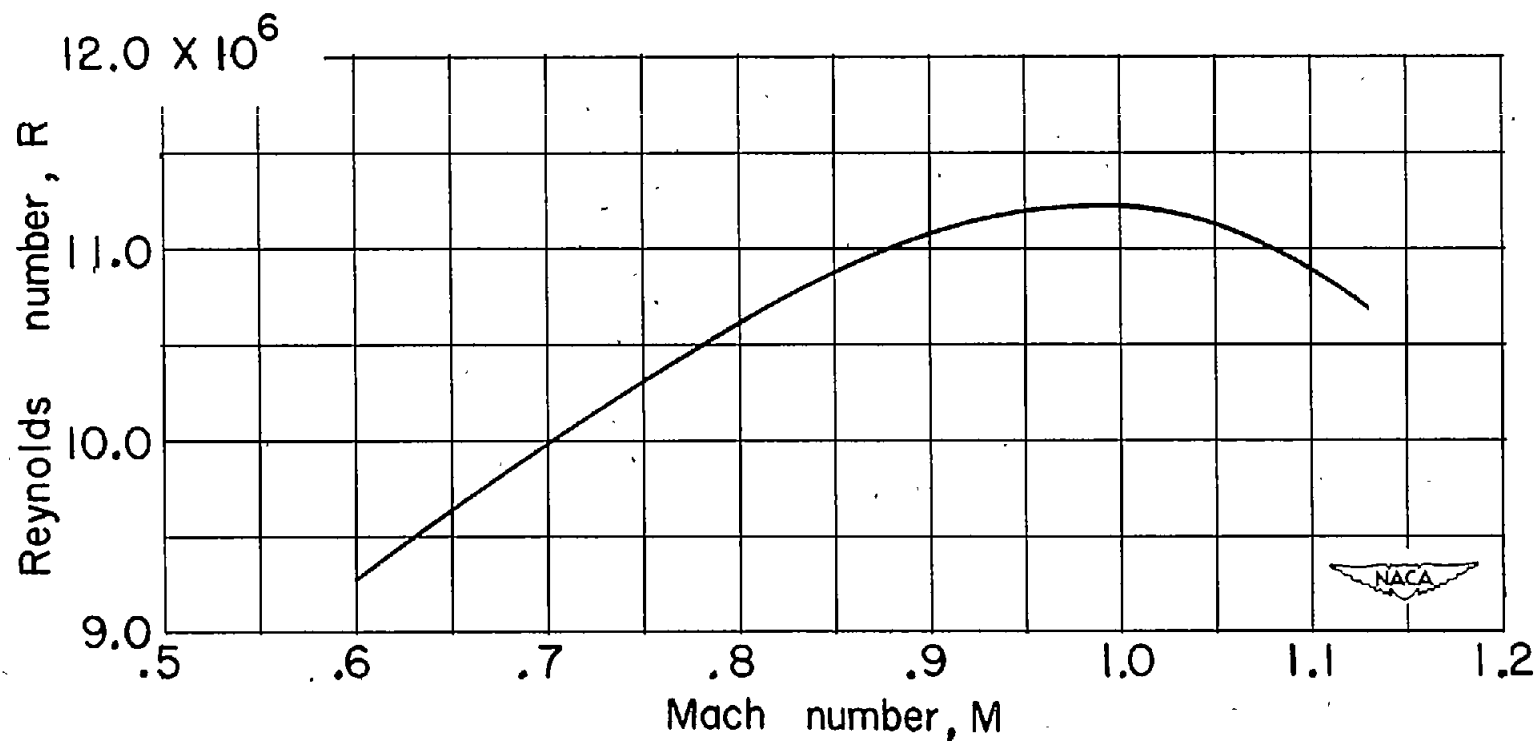


Figure 3.- Variation with Mach number of average test Reynolds number based on total body length of 33.333 inches.

3B

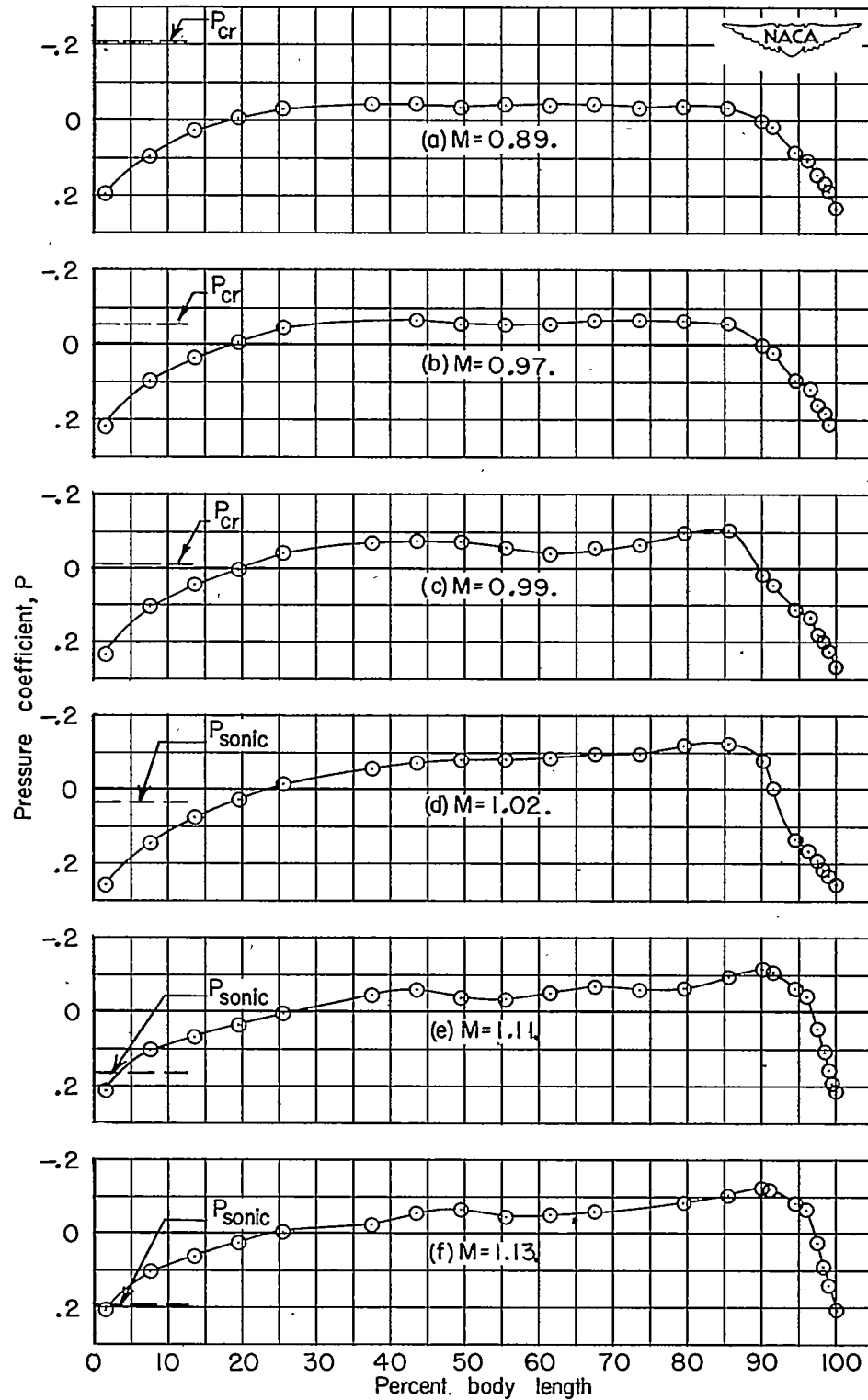


Figure 4.- Longitudinal pressure distribution for body of revolution at zero angle of attack for several Mach numbers.

CONFIDENTIAL

CONFIDENTIAL

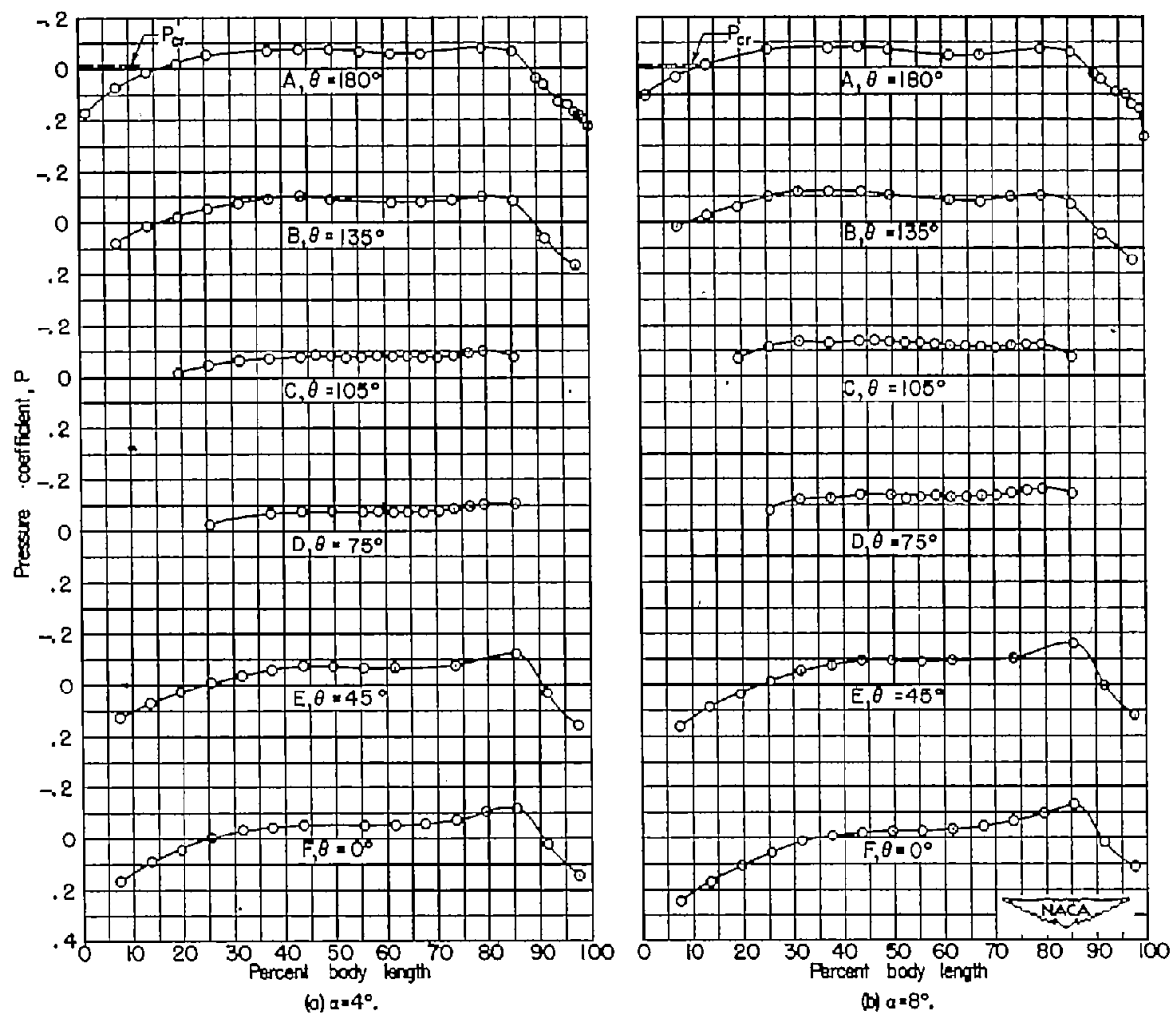


Figure 5.- Longitudinal pressure distribution at six radial locations for body of revolution at several angles of attack. $M = 0.99$.

CONFIDENTIAL

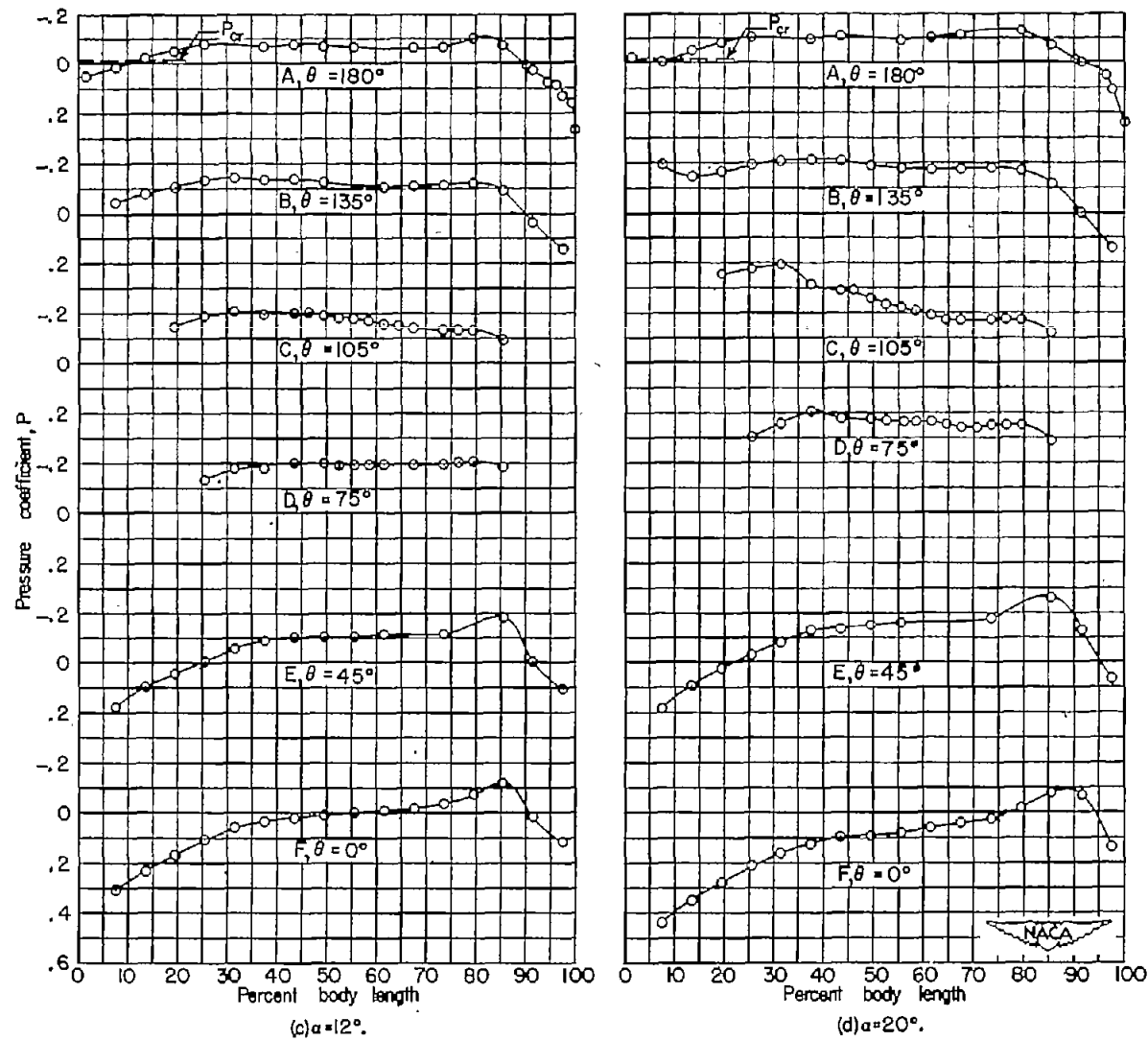


Figure 5.- Concluded.

CONFIDENTIAL

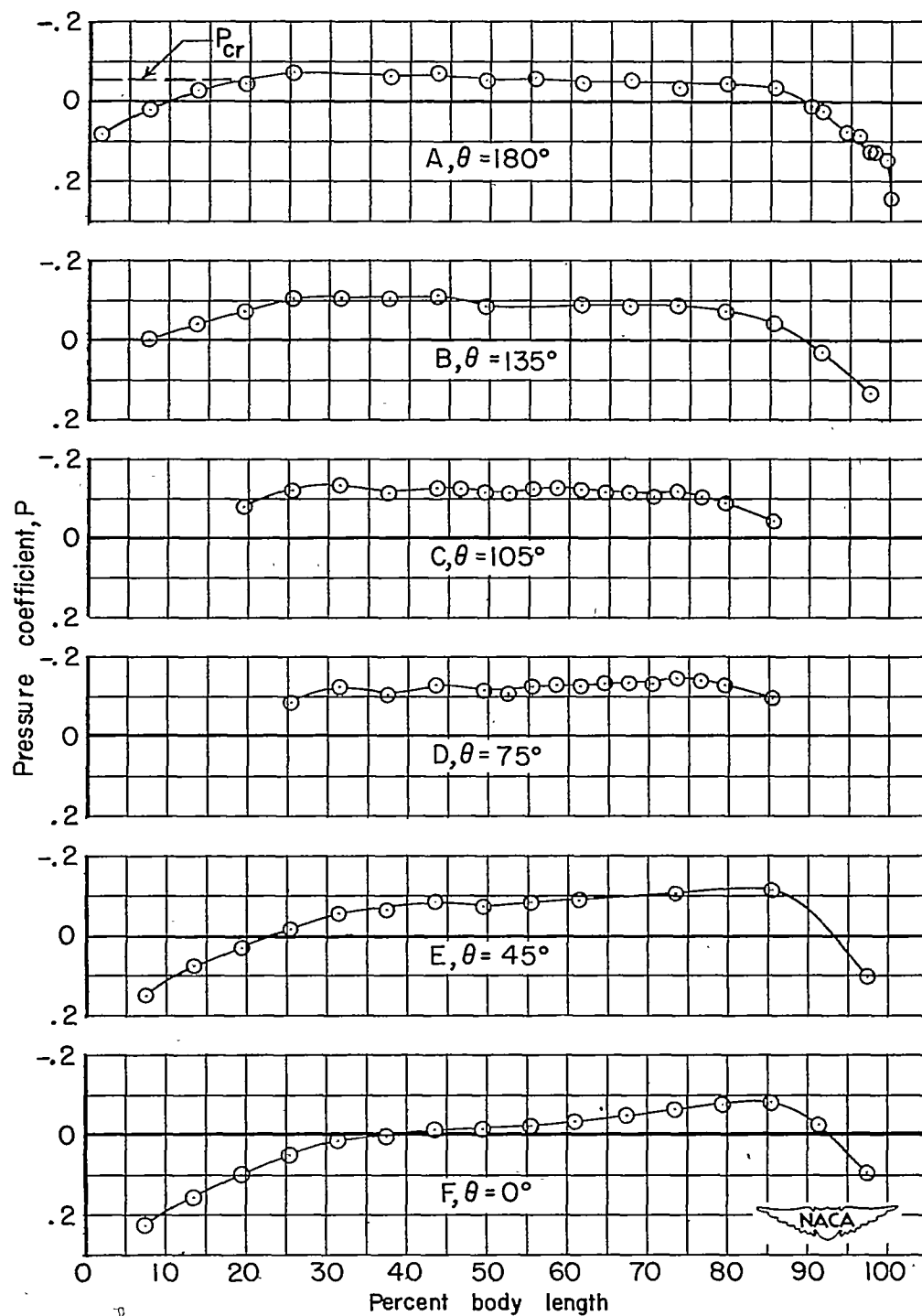
(a) $M = 0.97$.

Figure 6.- Longitudinal pressure distributions at six radial locations for body of revolution at several Mach numbers. $\alpha = 8^\circ$.

CONFIDENTIAL

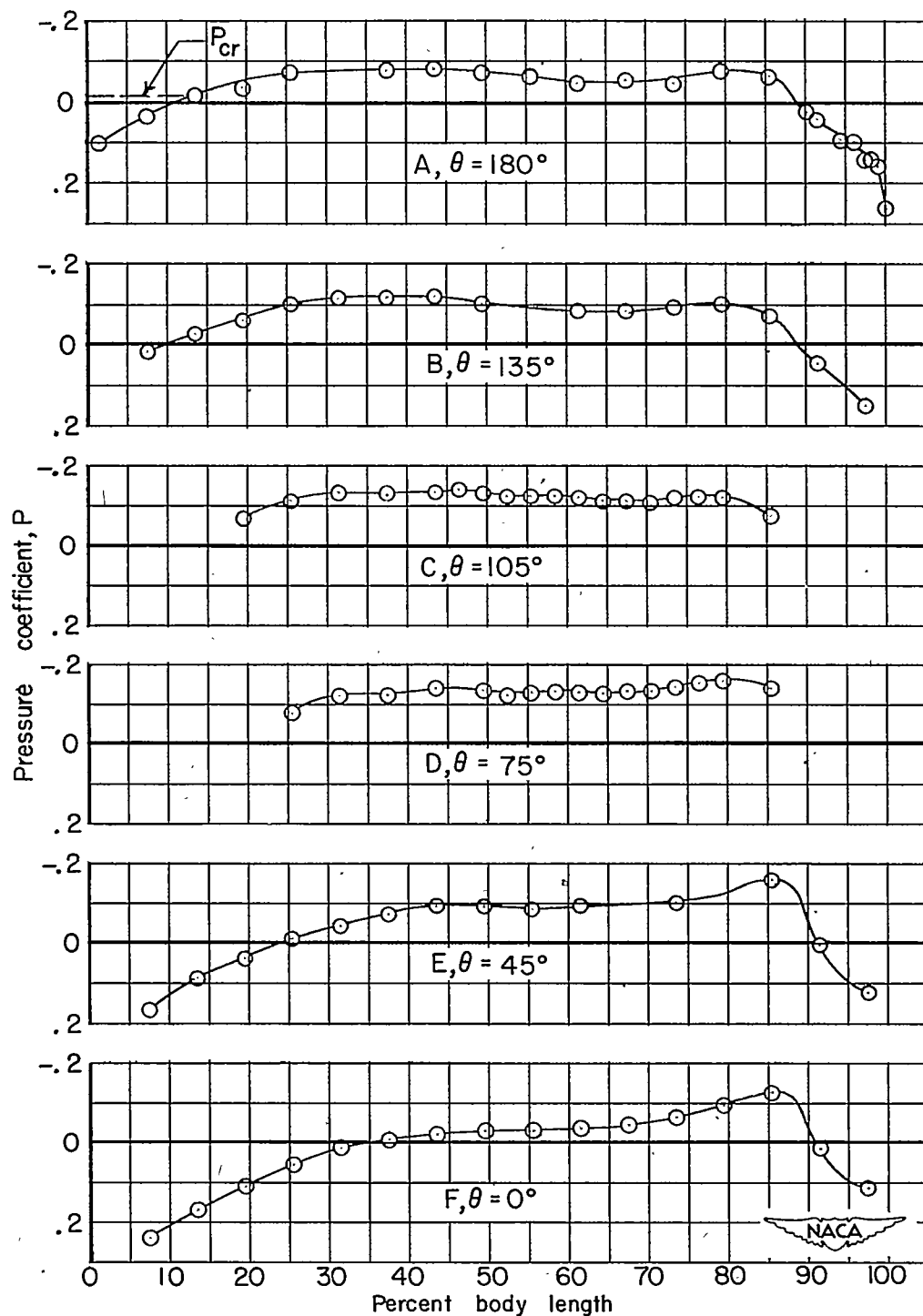
(b) $M = 0.99$.

Figure 6.- Continued.

CONFIDENTIAL

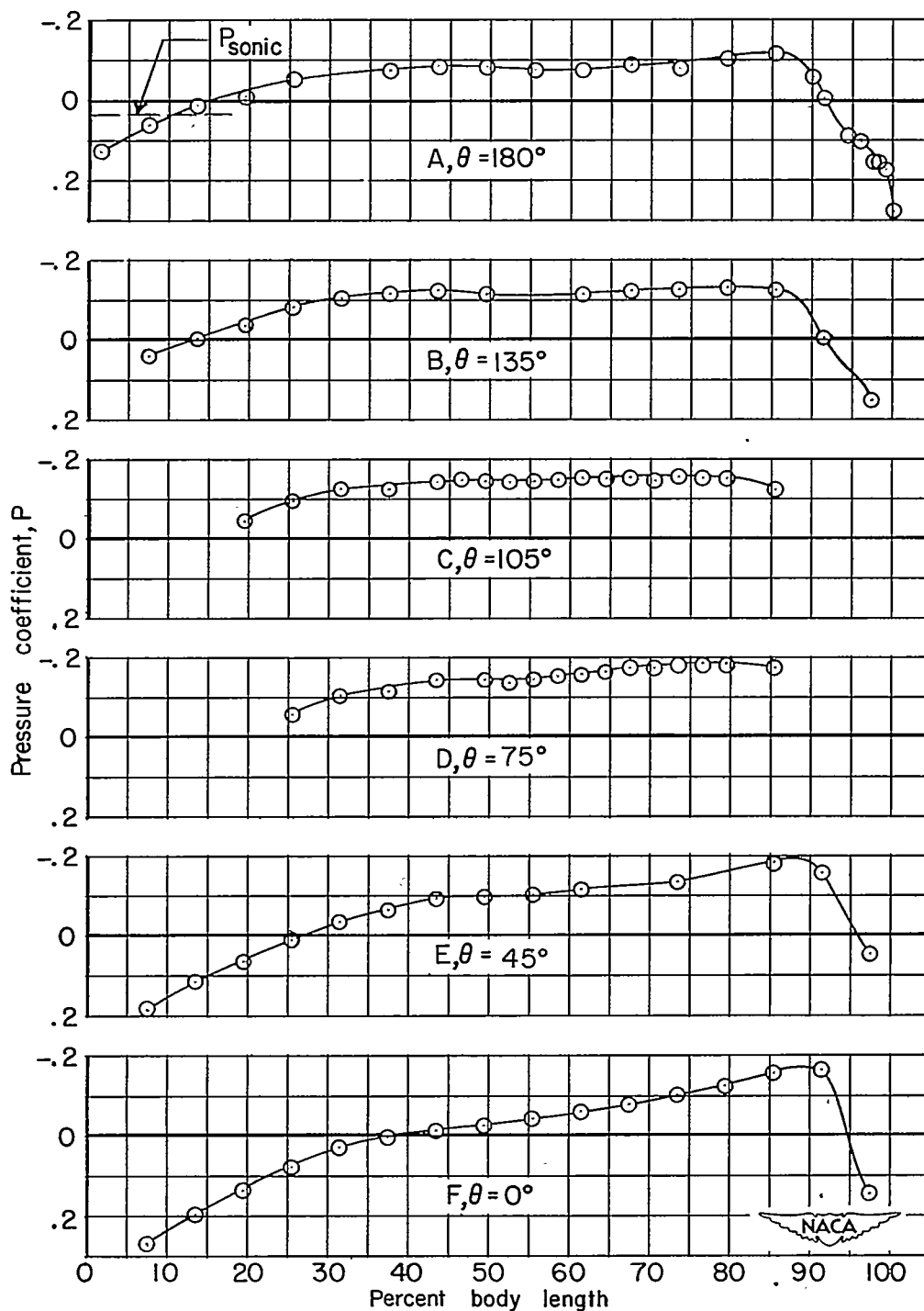
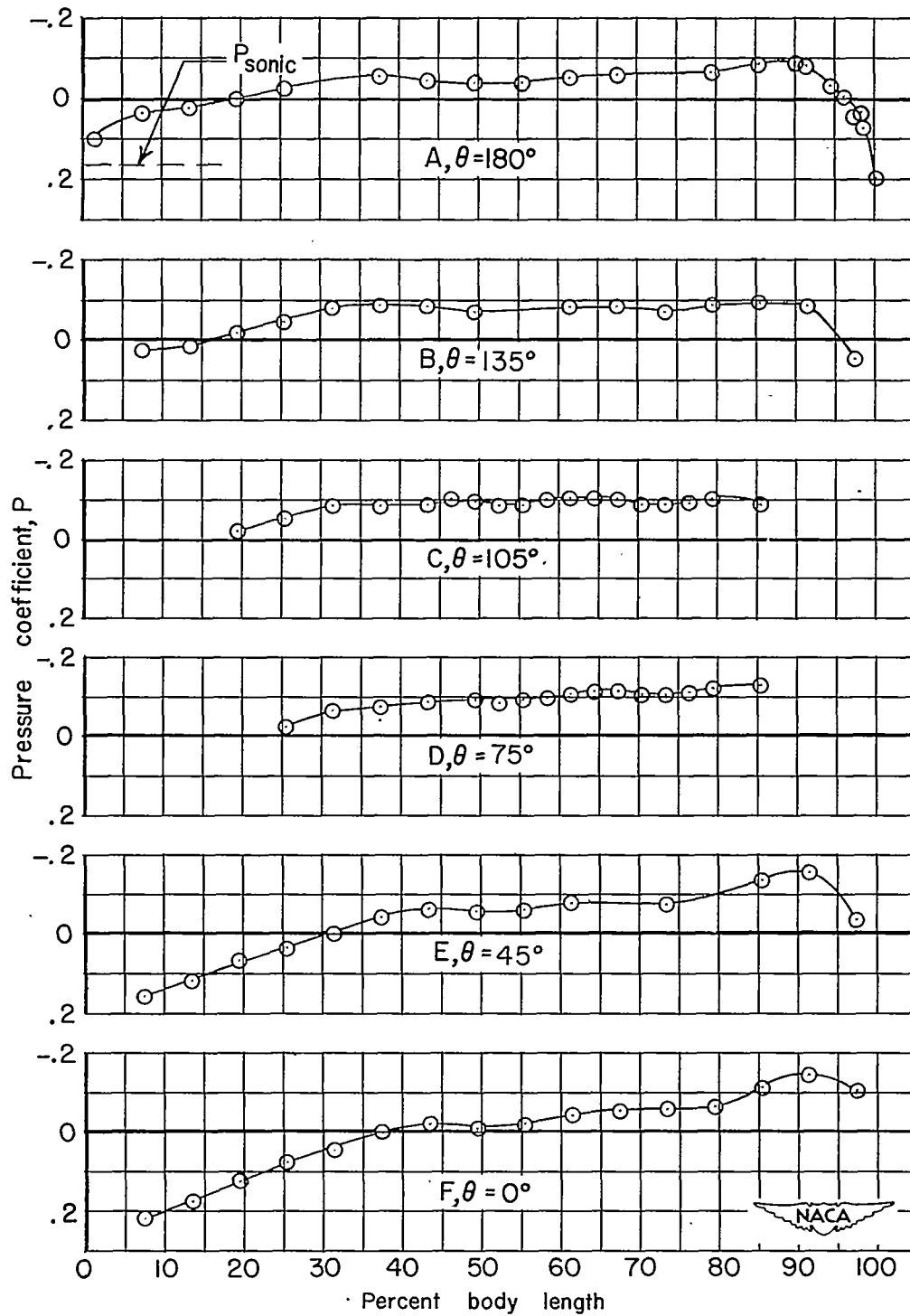
(c) $M = 1.02$.

Figure 6.- Continued.

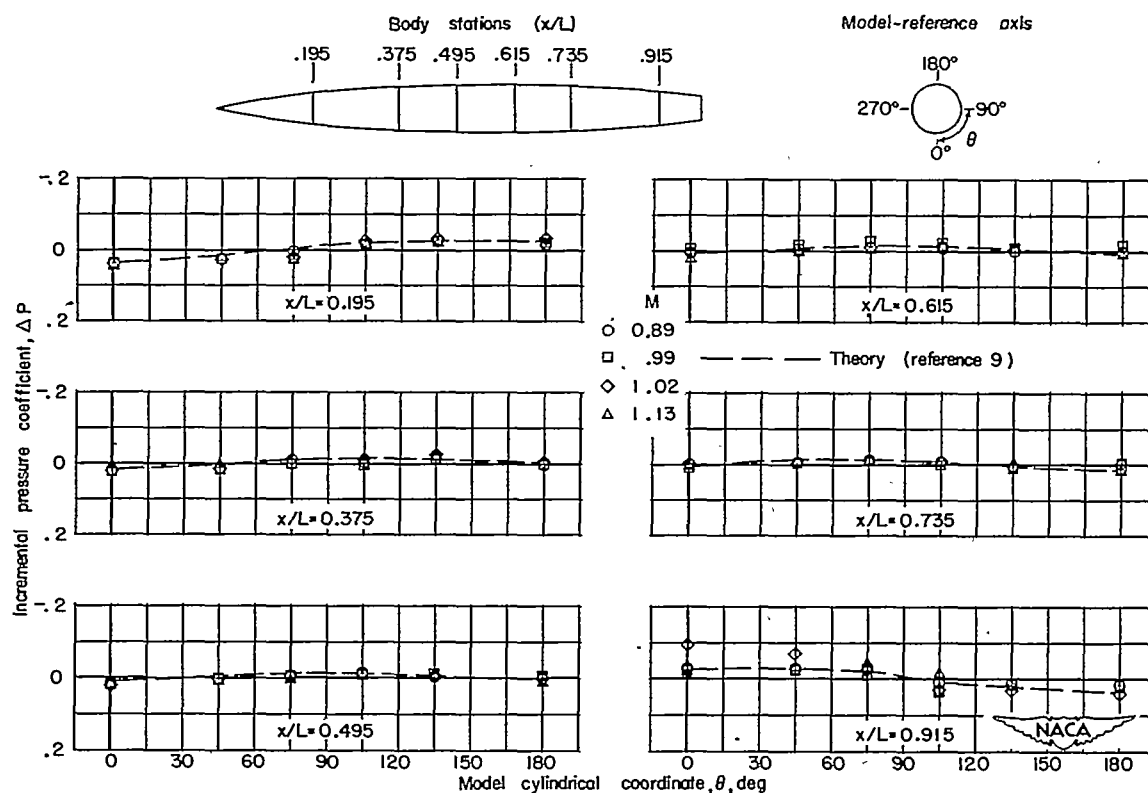
CONFIDENTIAL



(d) $M = 1.11$.

Figure 6.- Concluded.

CONFIDENTIAL



(a) $\alpha = 4^\circ$.

Figure 7.- Theoretical and experimental variation with angular position on body of pressure coefficient due to angle of attack for several Mach numbers.

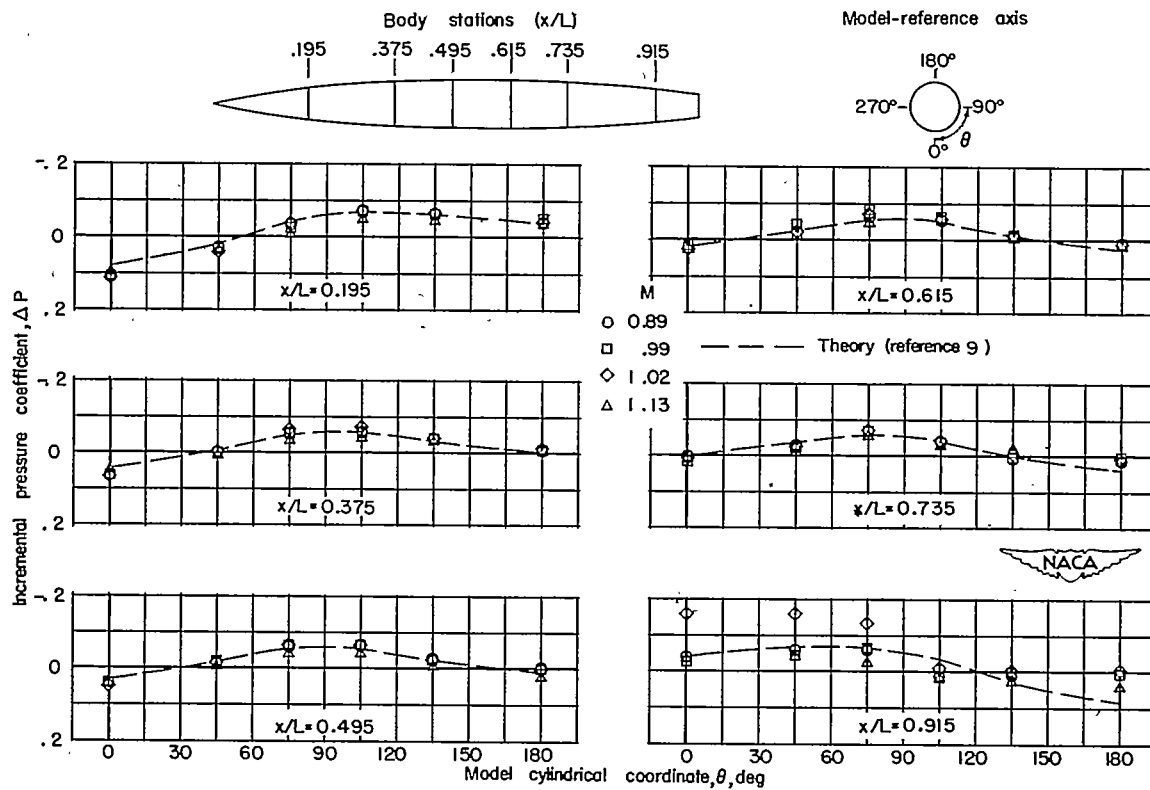
(b) $\alpha = -8^\circ$.

Figure 7.- Continued.

CONFIDENTIAL

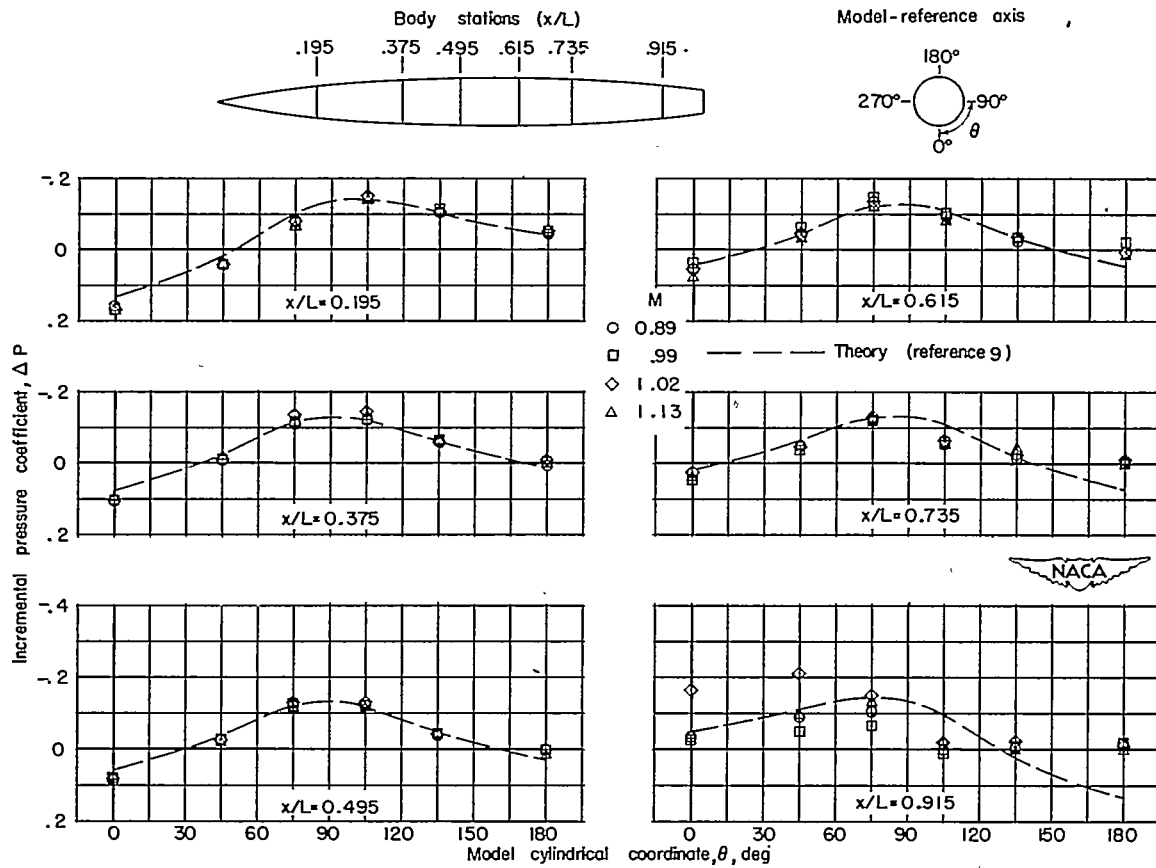
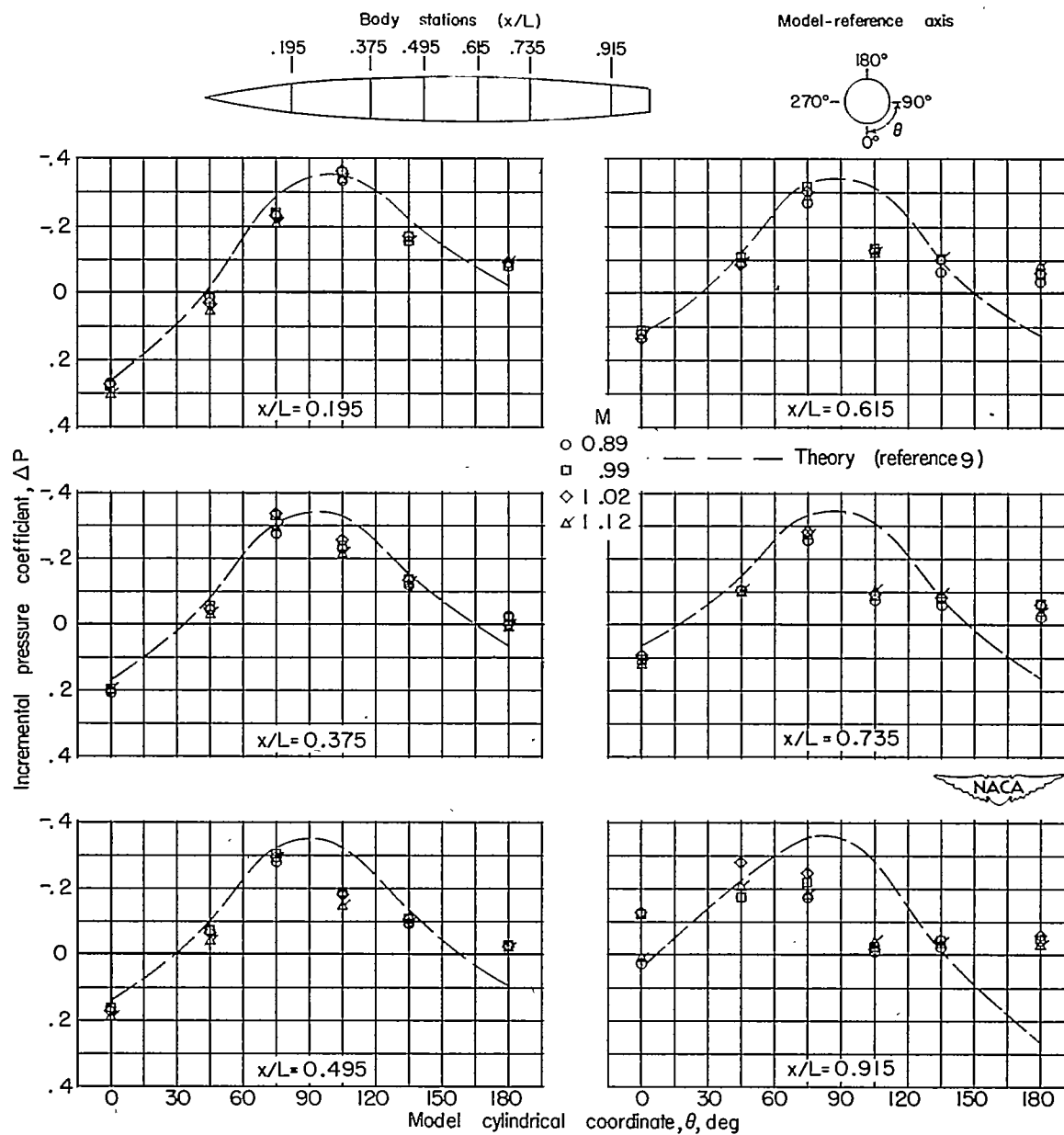
(c) $\alpha = 12^\circ$.

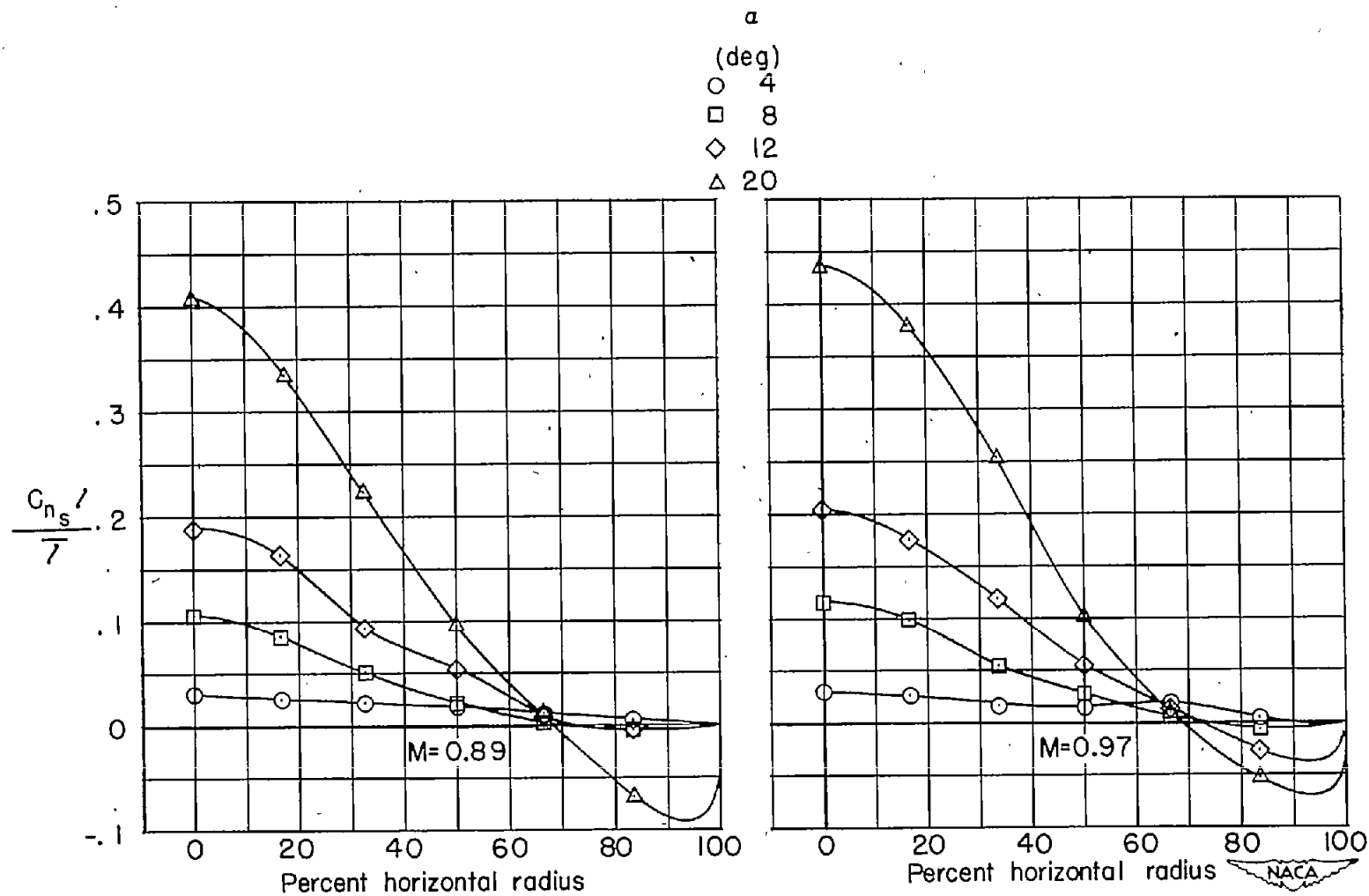
Figure 7.- Continued.

CONFIDENTIAL



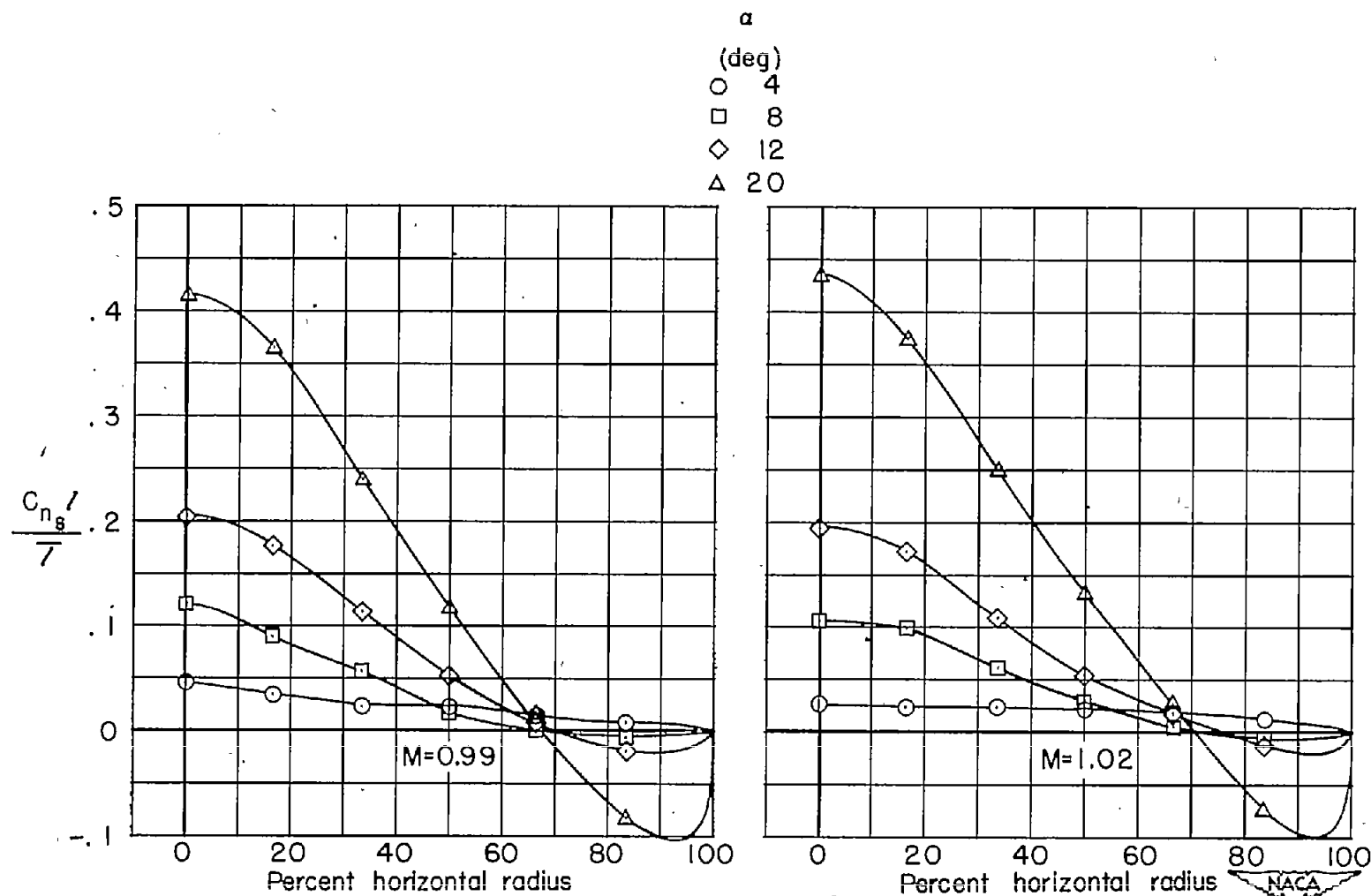
(d) $\alpha = 20^\circ$.

Figure 7.- Concluded.



(a) $M = 0.89$ and 0.97 .

Figure 8.- Lateral load distribution over body for several angles of attack.



(b) $M = 0.99$ and 1.02 .

Figure 8.- Continued.

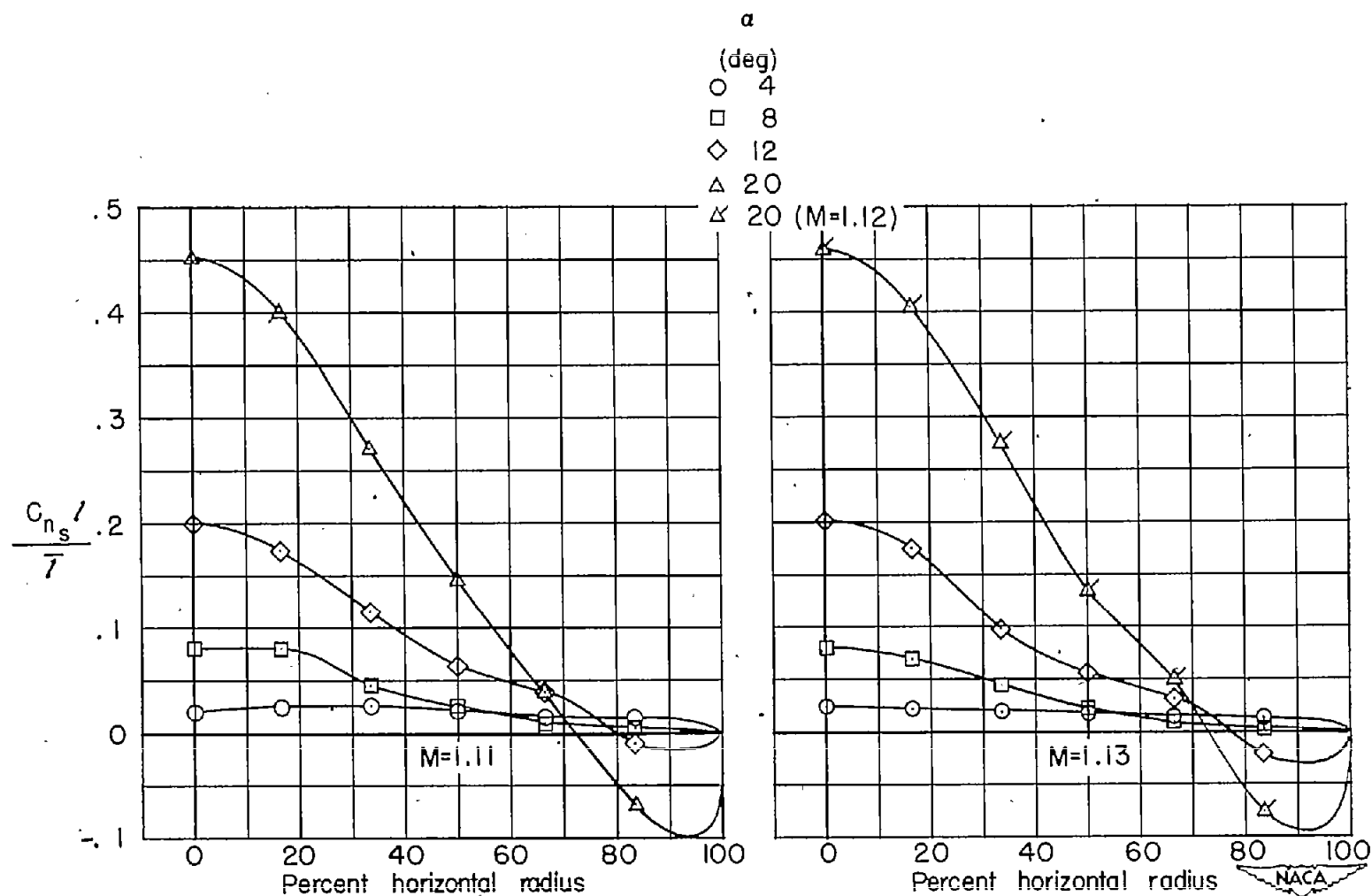
(c) $M = 1.11$ and 1.13 .

Figure 8.- Concluded.

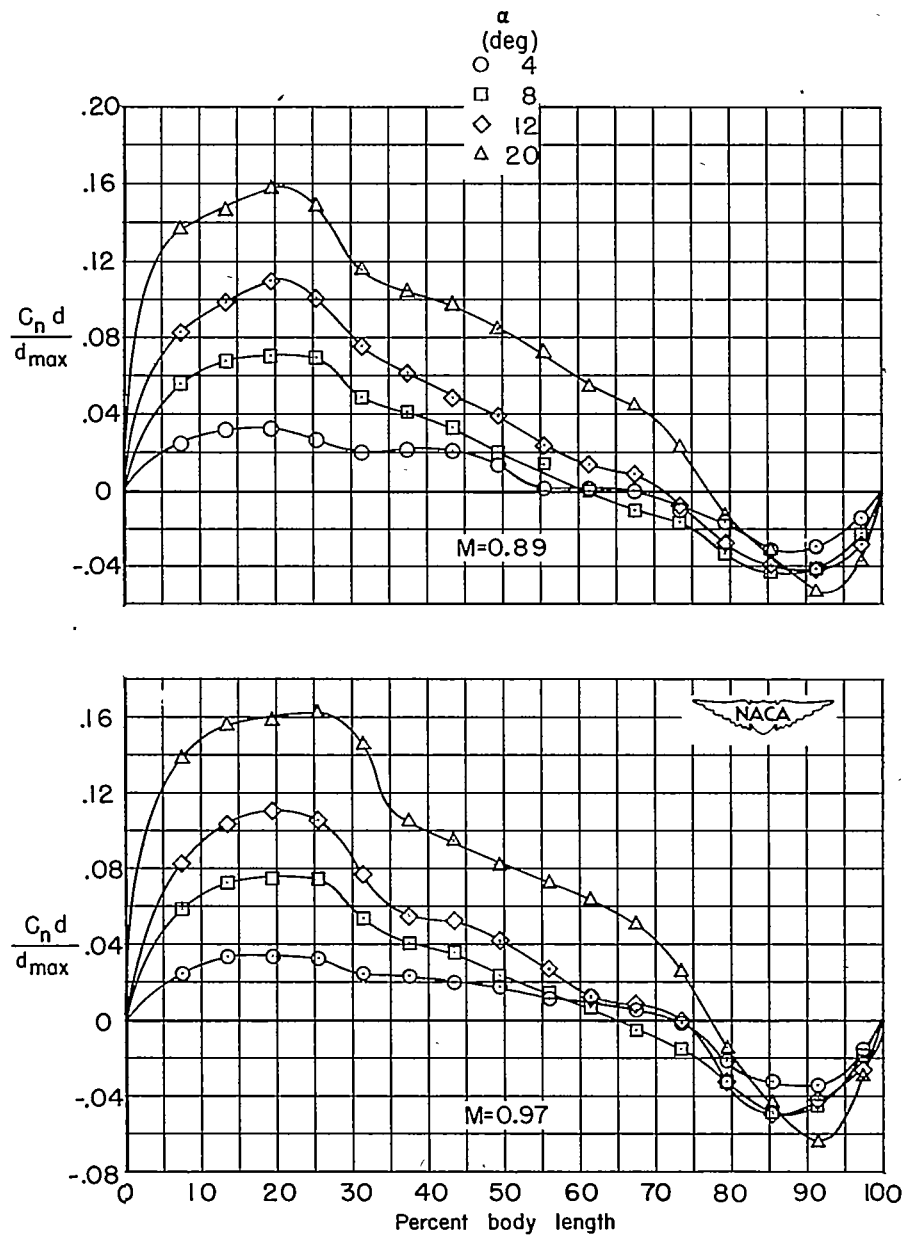
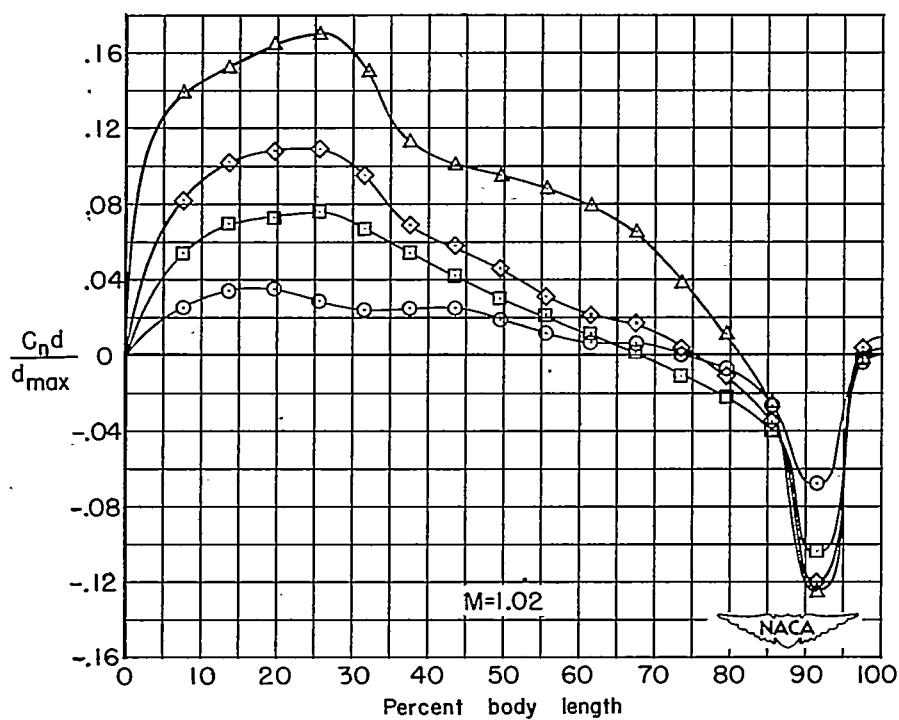
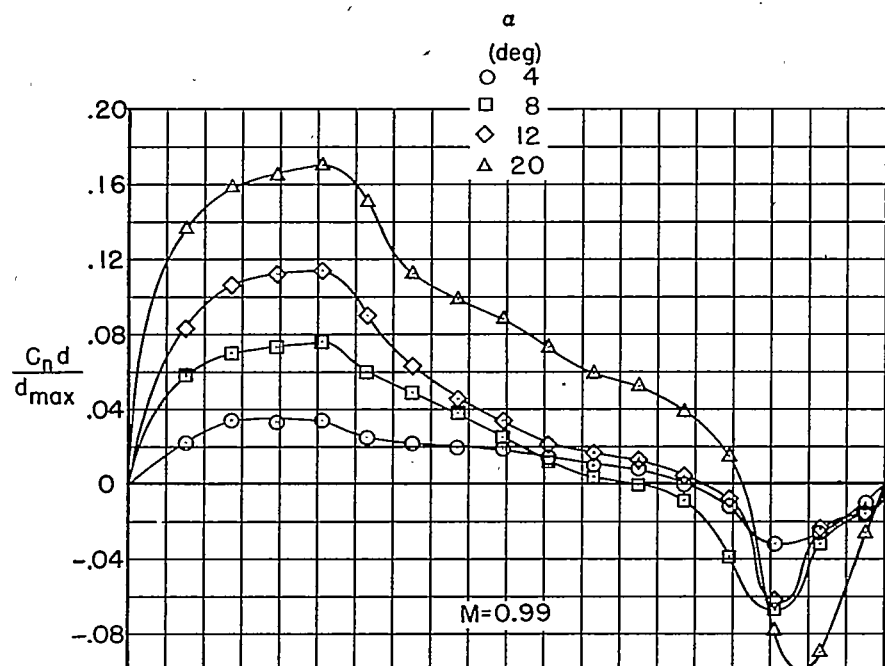
(a) $M = 0.89$ and 0.97 .

Figure 9.- Longitudinal load distribution over body for several angles of attack.



(b) $M = 0.99$ and 1.02 .

Figure 9.- Continued.

5B

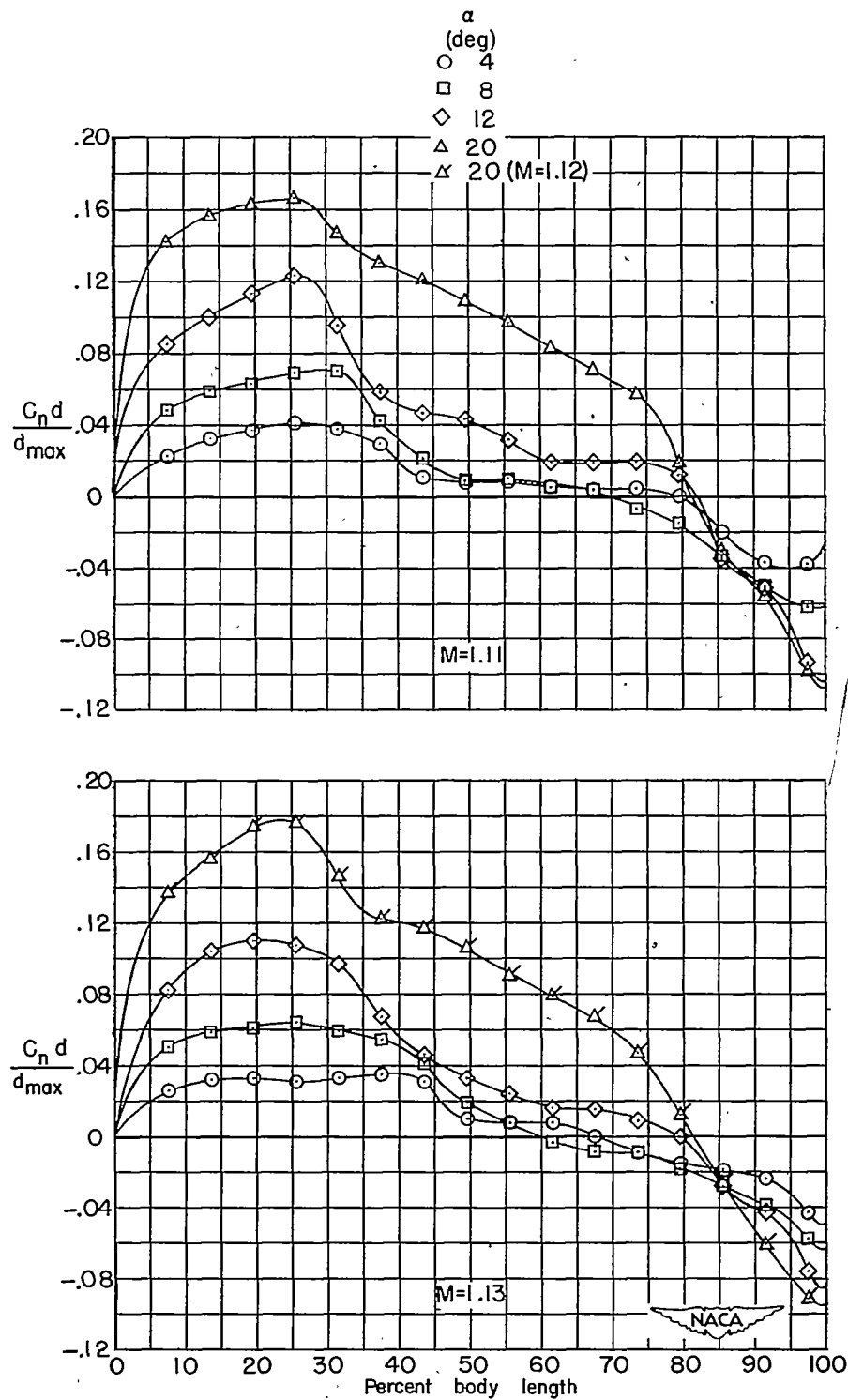
(c) $M = 1.11$ and 1.13 .

Figure 9.- Concluded.

CONFIDENTIAL

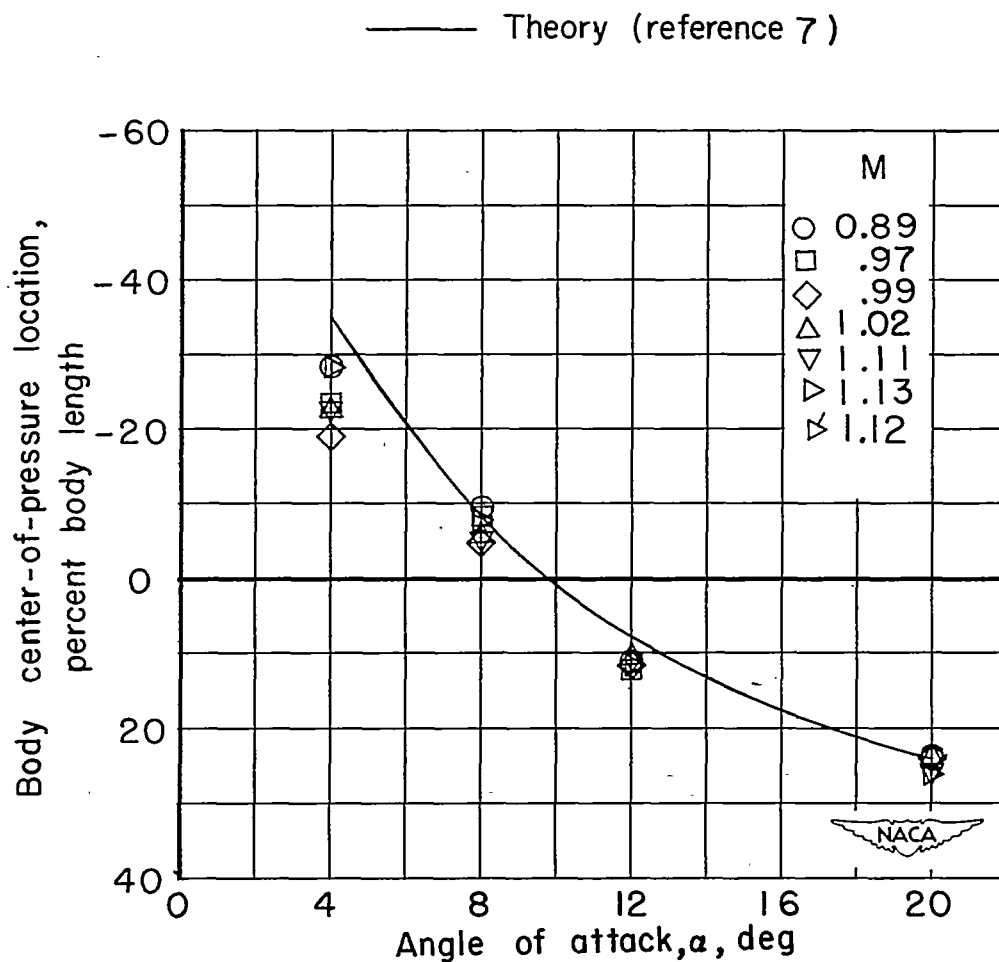
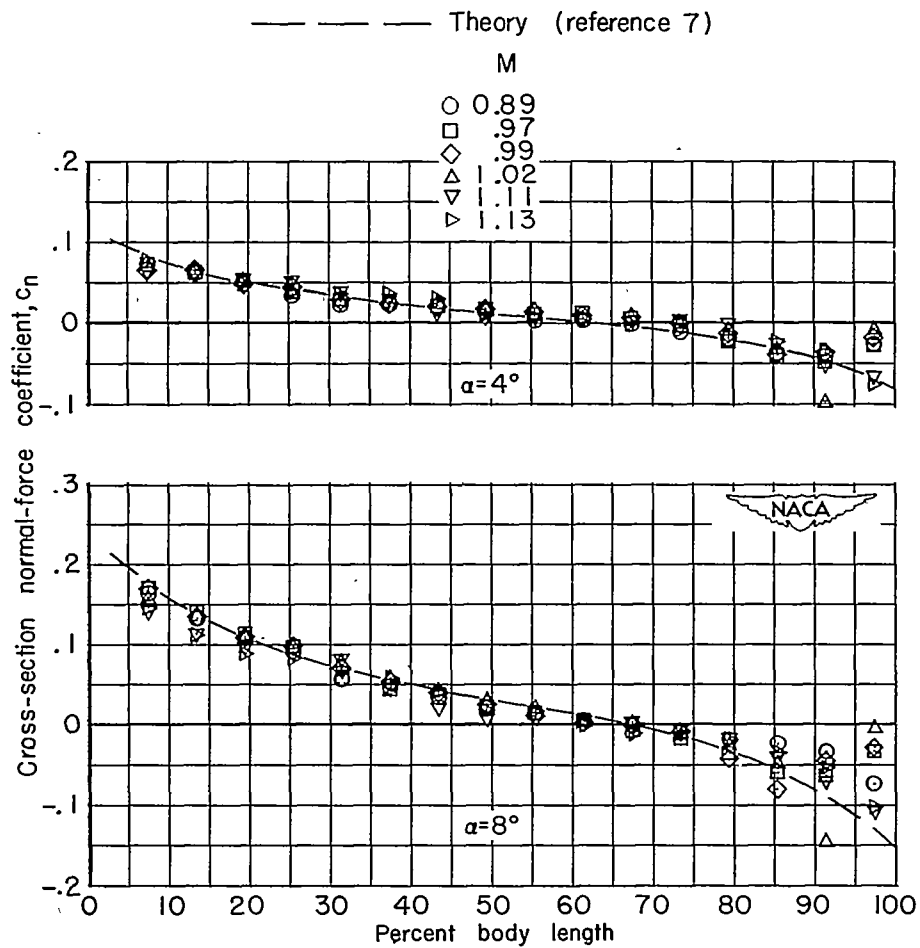


Figure 10.- Theoretical and experimental variation with angle of attack of body center of pressure for several Mach numbers.

CONFIDENTIAL



(a) $\alpha = 4^\circ$ and 8° .

Figure 11.- Cross-section normal-force distribution over the body for several Mach numbers.

CONFIDENTIAL

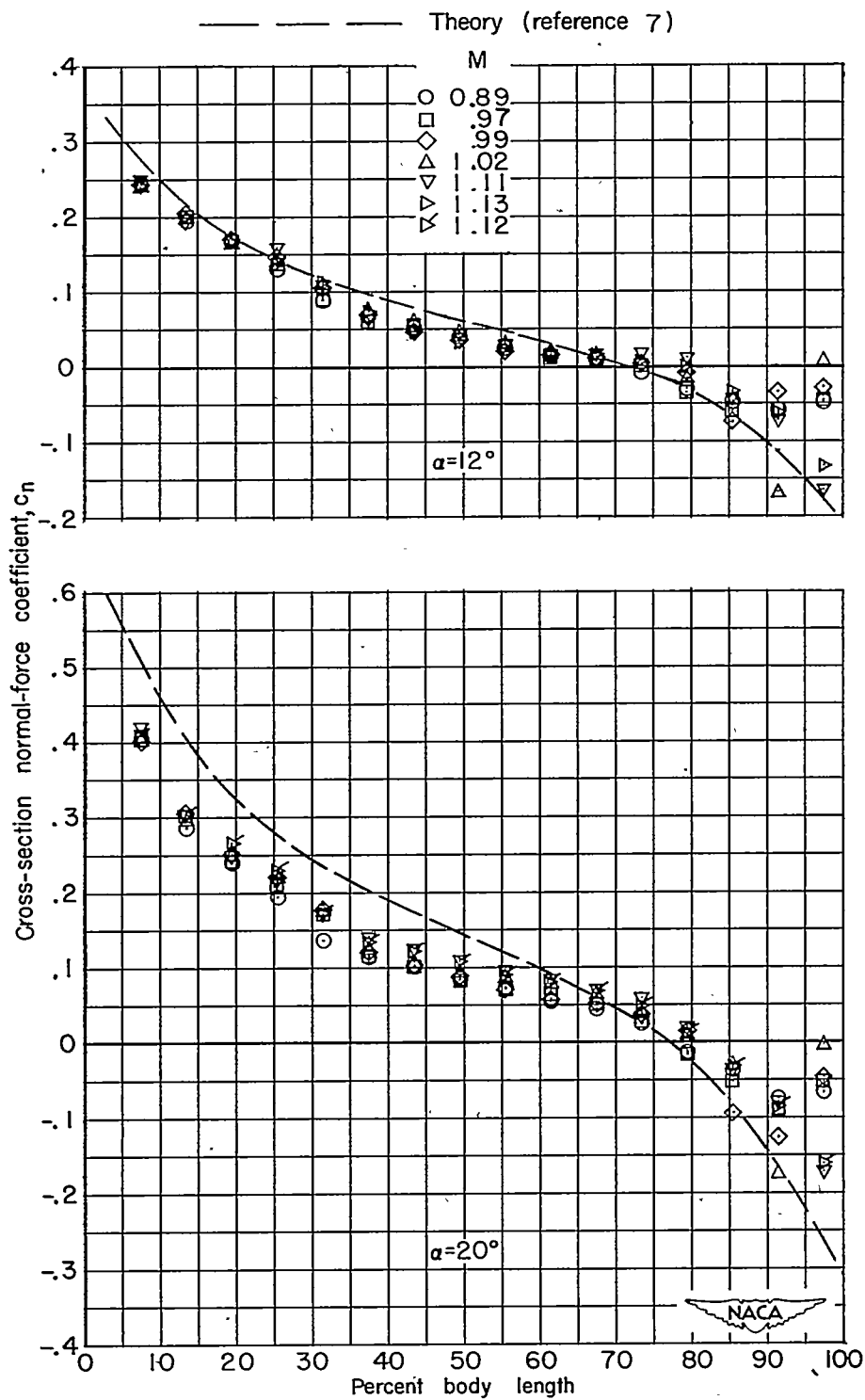
(b) $\alpha = 12^\circ$ and 20° .

Figure 11.- Concluded.

CONFIDENTIAL

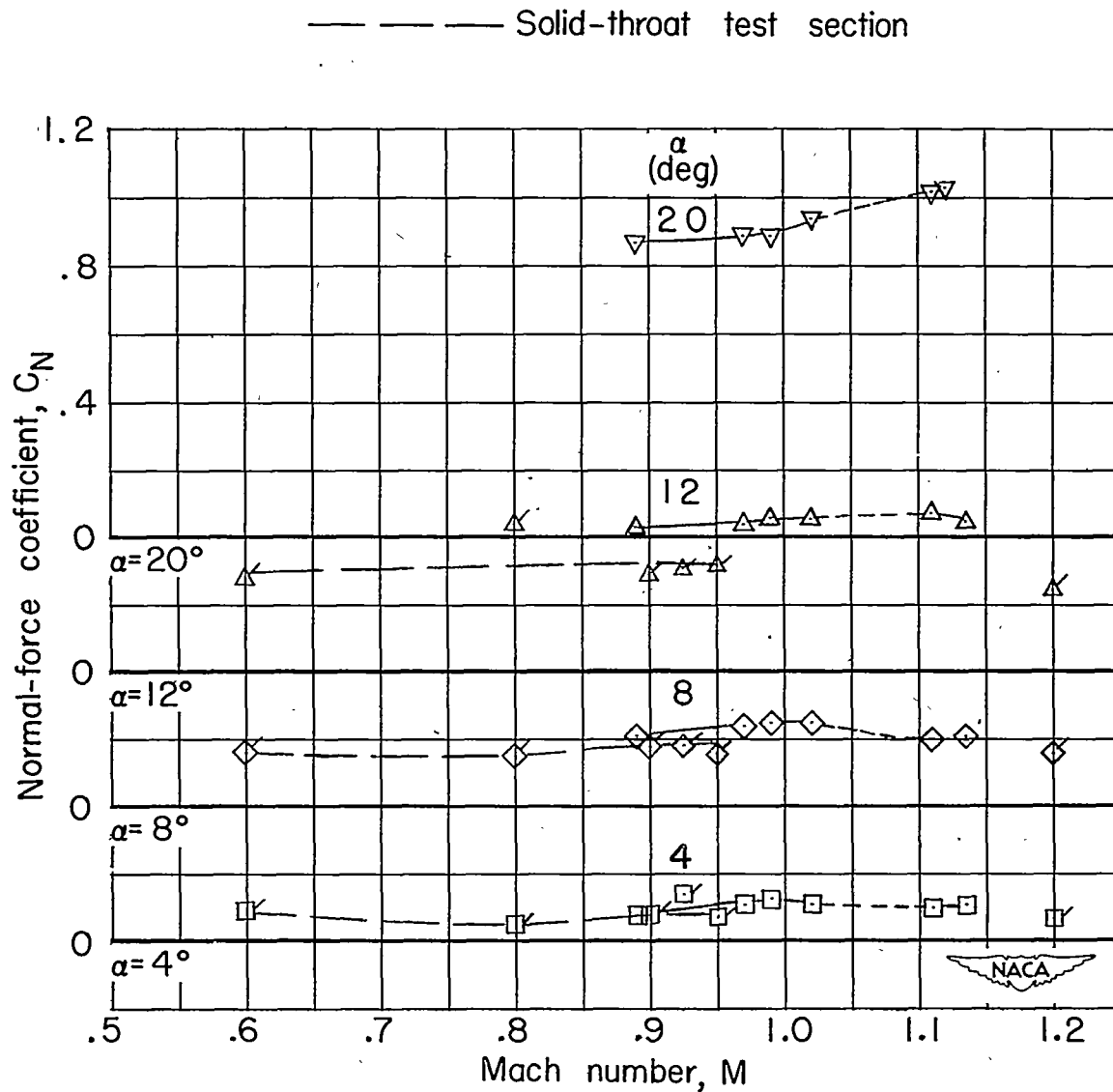


Figure 12.- Variation with Mach number of normal-force coefficient. (Plain symbols indicate pressure data from slotted throat test section; symbols with flags indicate pressure data from solid throat test section.)

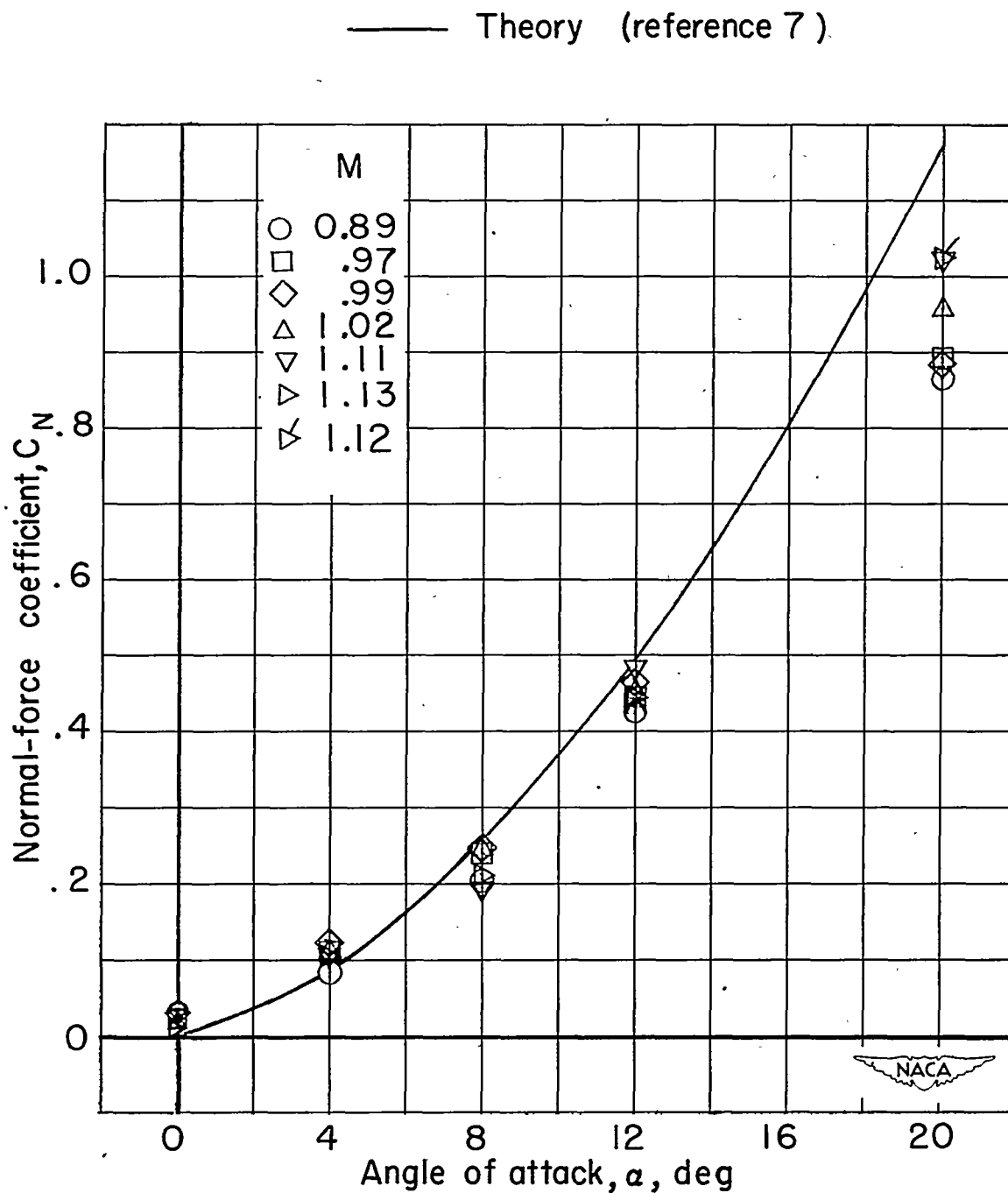
~~CONFIDENTIAL~~

Figure 13.- Theoretical and experimental variation with angle of attack of normal-force coefficient for several Mach numbers.

~~CONFIDENTIAL~~

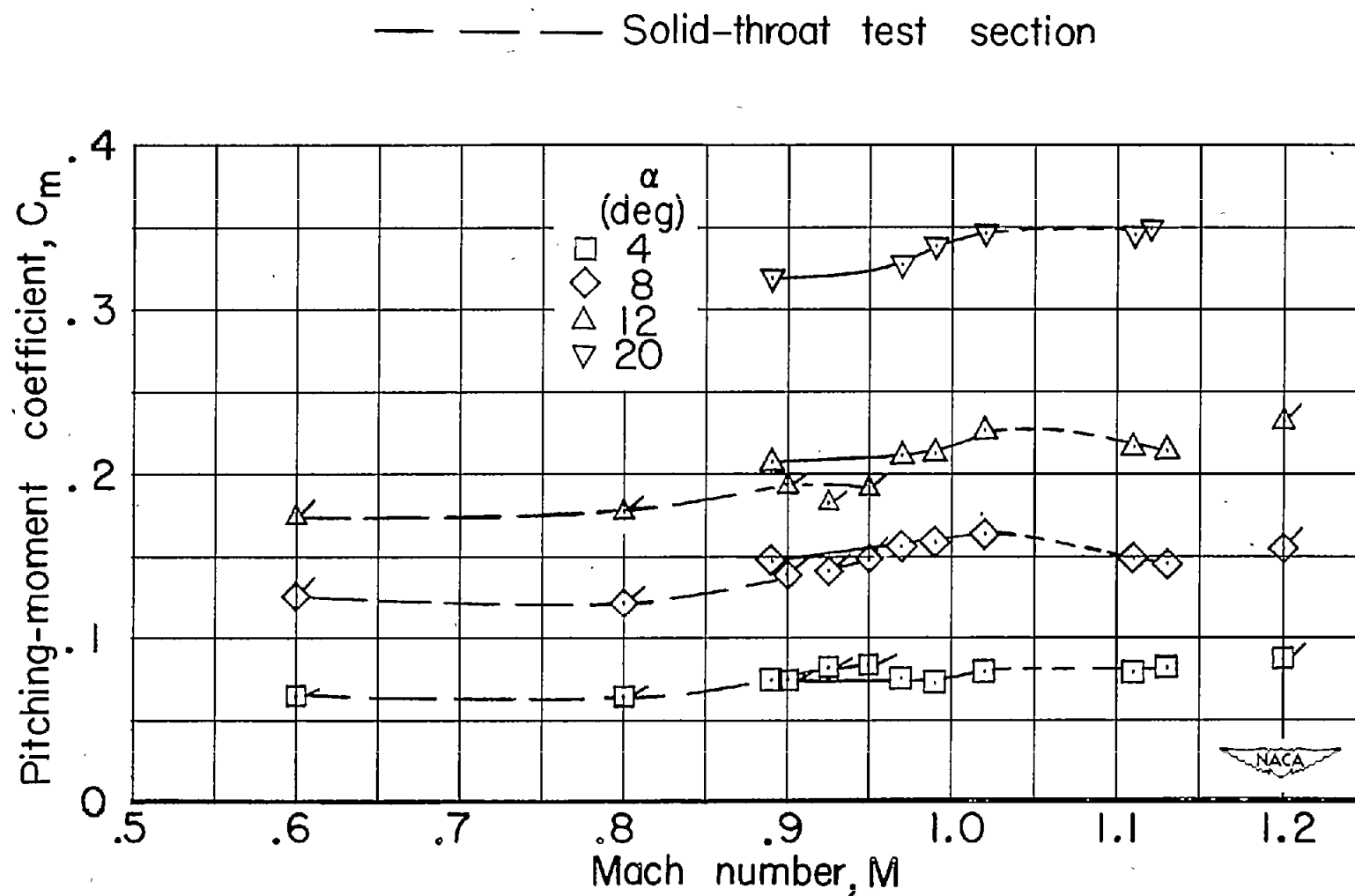


Figure 14.- Variation with Mach number of pitching-moment coefficient.
 (Plain symbols indicate pressure data from slotted throat test section;
 symbols with flags indicate pressure data from solid throat test section.)

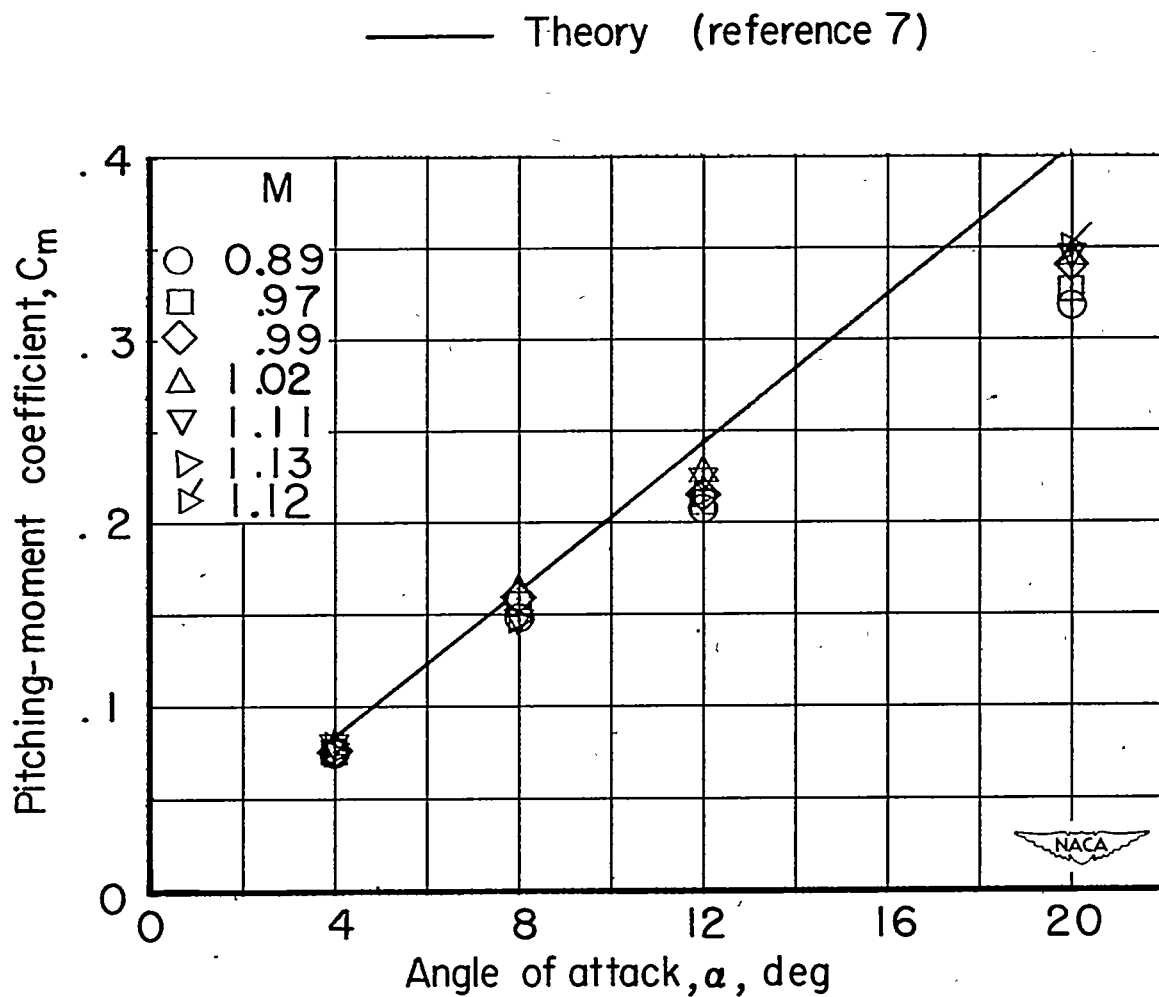


Figure 15.- Theoretical and experimental variation with angle of attack of pitching-moment coefficient for several Mach numbers.

CONFIDENTIAL

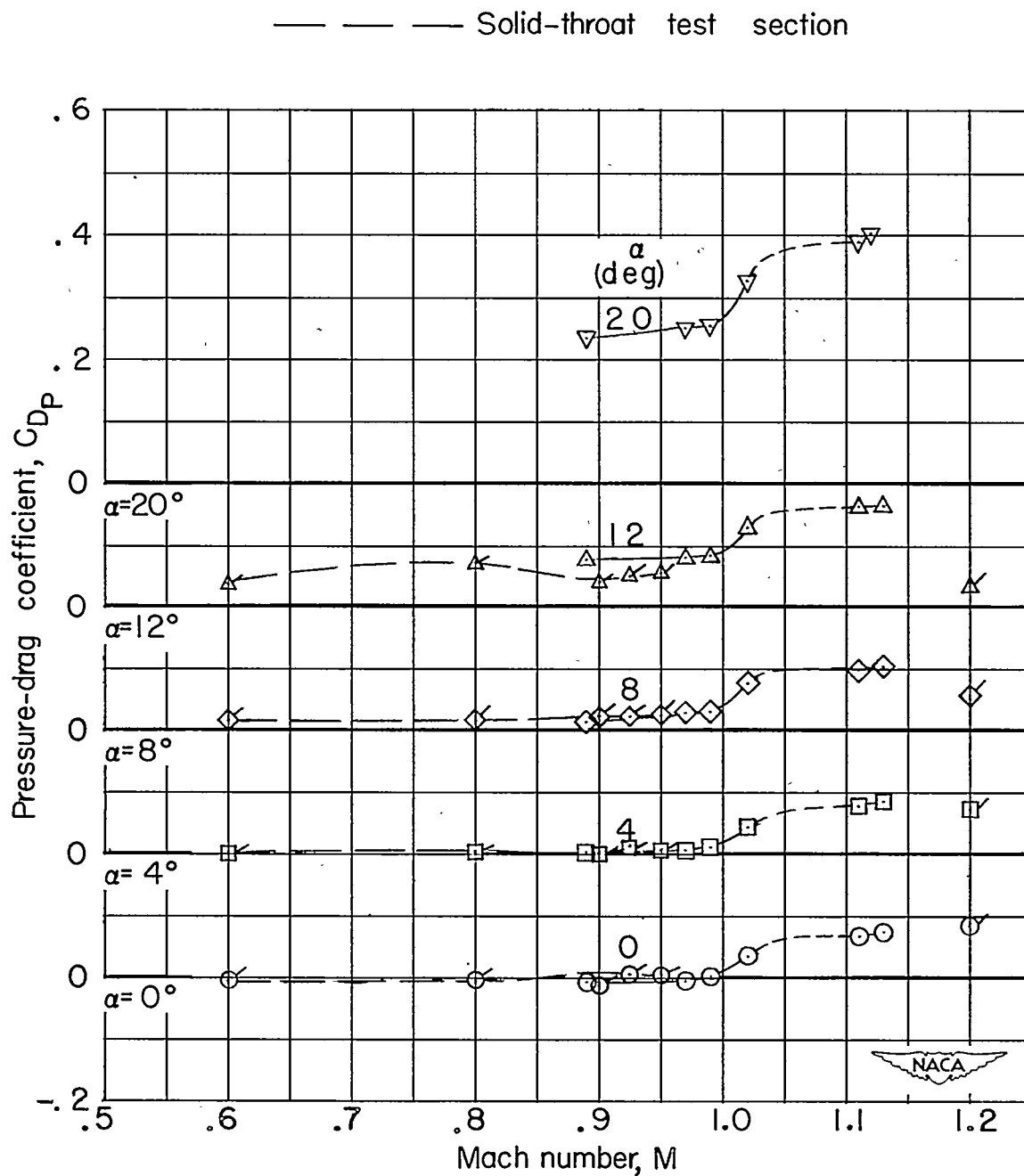


Figure 16.- Variation with Mach number of pressure-drag coefficient.
 (Plain symbols indicate pressure data from slotted throat test section; symbols with flags indicate pressure data from solid throat test section.)

CONFIDENTIAL

CONFIDENTIAL

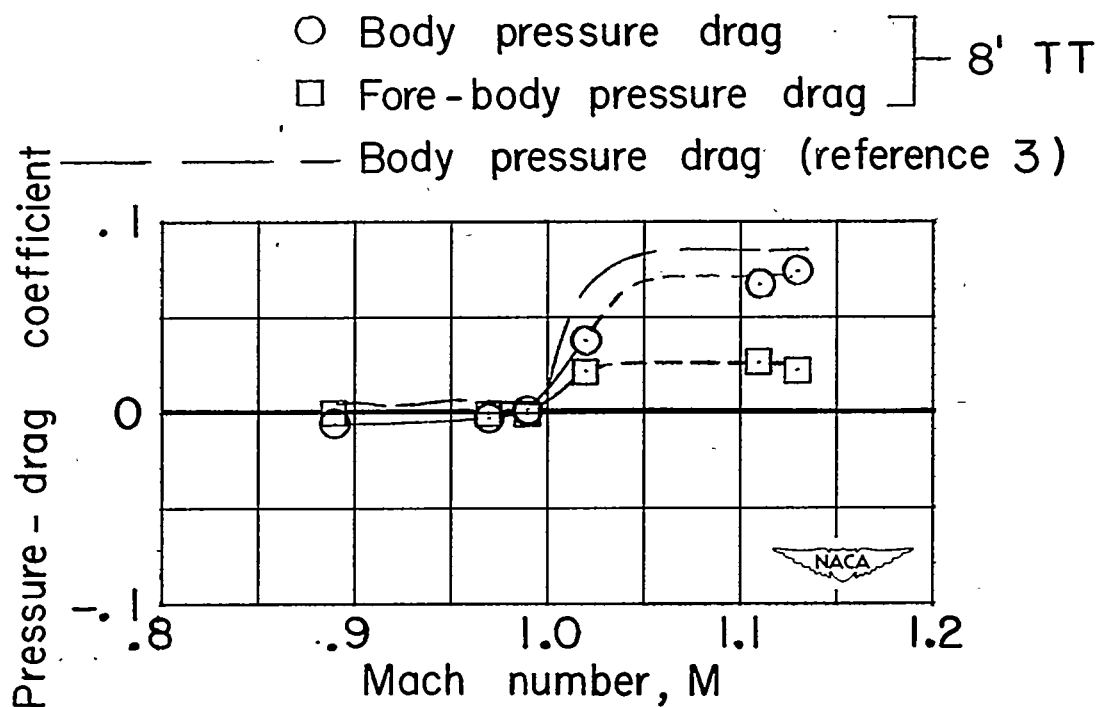


Figure 17.- Comparison of variation with Mach number of pressure-drag coefficient at zero lift for the body and a free-fall model..

CONFIDENTIAL